QUANTUM WAVE PACKET TRANSFORMS WITH COMPACT FREQUENCY SUPPORT

HONGKANG NI AND LEXING YING

ABSTRACT. Different kinds of wave packet transforms are widely used for extracting multi-scale structures in signal processing tasks. This paper introduces the quantum circuit implementation of a broad class of wave packets, including Gabor atoms and wavelets, with compact frequency support. Our approach operates in the frequency space, involving reallocation and reshuffling of signals tailored for manipulation on quantum computers. The resulting implementation is different from the existing quantum algorithms for spatially compactly supported wavelets and can be readily extended to quantum transforms of other wave packets with compact frequency support.

1. Introduction

Various types of wave packets, such as wavelets [Mal99], Gabor atoms, curvelets [CD05], wavelet packets [LM04], and wave atoms [DY07], have been extensively explored and applied to many applications. In contrast to the Fourier and the Dirac bases, these wave packets exhibit locality in both the spatial and frequency domains, along with a controlled level of smoothness, making them advantageous for image or other signal processing tasks. Additionally, research has demonstrated that the structure of these wave packet bases offers sparse representations for some differential operators, enabling their use as effective preconditioners for partial differential equations and facilitating the development of rapid algorithms [CD03, DY09].

There has been emerging interest in quantum algorithms utilizing wavelet or other wave packet transformations. Research works have demonstrated the applicability of quantum wavelet transforms in various areas of image processing [YIVA16, ZYI⁺22], including image compression and encryption [ZHGZ20], image denoising [CSCG20], and image watermarking [YGMW23, SWL⁺13, MWB⁺23, HNG⁺17]. Furthermore, quantum wavelet transform has found applications in diverse fields such as quantum steganography [GZL22], quantum-to-classical data decoding [JUIL⁺23], and signal reconstruction [MBDJ20]. Notably, quantum wavelet and curvelet transforms have also been found valuable in encoding differential operators [KDPE⁺22, BNWAG23] and in the domain of quantum sampling [Liu09].

Similar to the Fourier transform, quantum computing presents the potential for exponential speedup for wave packet transforms. The implementations of various quantum wavelet transforms have been explored. Earlier studies included well-known wavelets such as the Haar wavelet and Daubechies D4 wavelet [FW99, LFXS19]. Research has been extended to higher-order wavelets [BAG23] and a more general setting [ZK22]. The exploration of multi-dimensional quantum wavelet transform has also been undertaken [LLX23, LFP⁺22, LFX⁺18]. Wavelet packet transforms have been addressed in studies like [Kla99, CGFUPSRG23]. However, there is a noticeable gap in research concerning other types of wave packet transforms. [Liu09] touched upon the multi-dimensional curvelet transform and its potential applications, but the discussion remains somewhat conceptual without a detailed exploration of its implementation.

1.1. Main contributions. Previous studies on quantum wavelet transforms have mostly utilized finite-size filters in the spatial domain, which are only applicable to spatially compactly supported wavelets. On the other hand, wave packet constructions with compact frequency support, such as the Meyer wavelet, exhibit favorable characteristics in the frequency domain. As far as we know, no existing algorithm has explored their

²⁰²⁰ Mathematics Subject Classification. 81P68, 68Q12, 42C40, 65T60.

Key words and phrases. Quantum algorithm, wavelet transform, Gabor atom, wave packet transform.

The work of L.Y. is partially supported by the National Science Foundation under awards DMS-2011699 and DMS-2208163.

implementations on quantum computers. Our contribution lies in operating within the frequency domain and executing the implementation of such wave packet constructions.

We first consider the Gabor atoms of uniform frequency partitioning, with both sharp and blended frequency windows. The implementation given here is the first one on quantum computers and also serves as a preparation for more advanced wave packets.

Next, we consider the wavelets of multiscale frequency partitioning with both sharp and blended frequency windows. The two examples studied in detail are Shannon wavelets and Meyer wavelets. We show that these wavelets may be realized with no more than three ancilla qubits, thanks to their favorable forms in the frequency domain. In contrast, for the wavelets with compact spatial support, the number of ancilla qubits typically grows with the order of the wavelet [BAG23].

1.2. Background on Gabor atoms and wavelets. Different tilings of phase-space diagrams result in different basis sets, which can be collectively called wave packets. This work focuses on two such wave packets: Gabor atoms and wavelets.

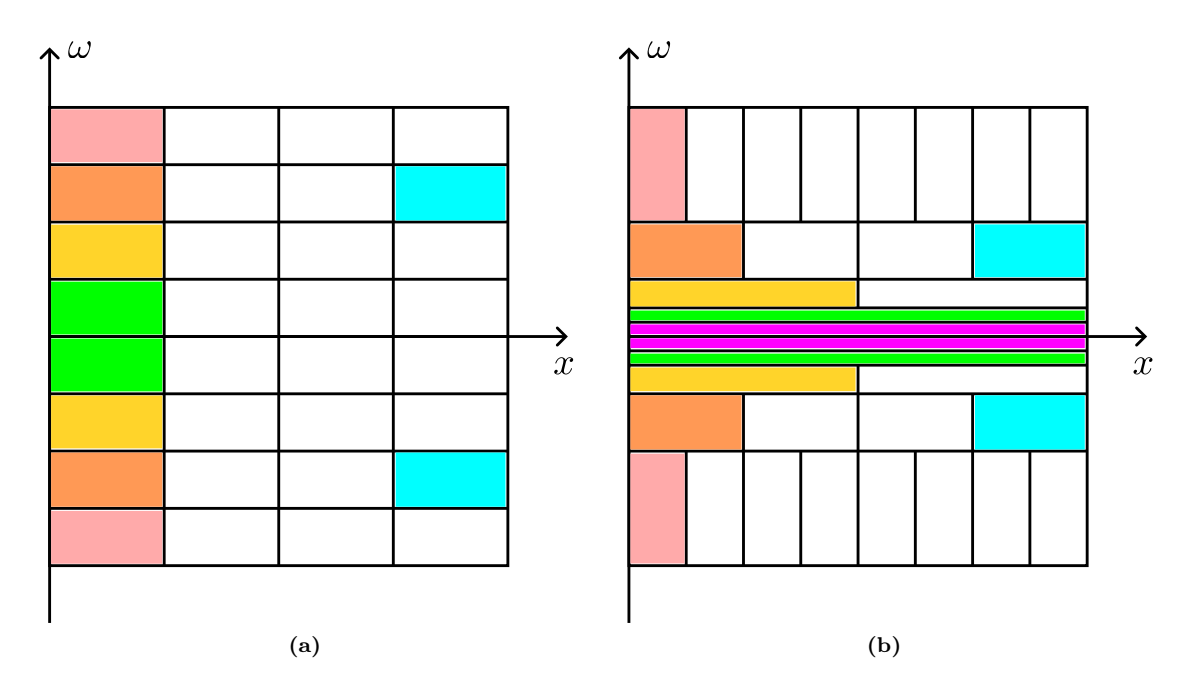


Figure 1. (a) Illustration for Gabor atom tiling. Each pair of tiles symmetric with respect to the x axis represents the essential support of a basis function $\psi_{j,p}$. The red, orange, yellow, and green tiles represent $\psi_{4,0}$, $\psi_{3,0}$, $\psi_{2,0}$, and $\psi_{1,0}$ respectively. All tiles with the same ω are at the same level j. For instance, the blue tile represents $\psi_{3,3}$. (b) Illustration for wavelet tiling. Each pair of tiles symmetric with respect to the x axis represents the essential support of a basis function $\psi_{j,p}$. This diagram shows the truncation up to n=4. The red, orange, yellow, green, and blue tiles represent $\psi_{1,0}$, $\psi_{2,0}$, $\psi_{3,0}$, $\psi_{4,0}$, and $\psi_{2,3}$ respectively. The purple tiles represent the scaling function.

1.2.1. Gabor atoms. Let us first consider a uniform phase-space tiling, as illustrated in Figure 1a. The basis functions given by this uniform tiling are called Gabor atoms. A basis function can be indexed by its frequency level $j \in \mathbb{Z}_{>0}$ and its space position $p \in \mathbb{Z}$. As the simplest example, the Gabor atoms with *sharp* frequency windows are given by

(1.1)
$$\widehat{\psi_{j,p}}(\omega) = \sqrt{\frac{A}{2\pi}} e^{iA\omega p} \chi_{\left[j\frac{\pi}{A},(j+1)\frac{\pi}{A}\right]}(|\omega|),$$

where χ stands for the indicator function. Here, we adopt the convention

$$\hat{\Psi}(\omega) = \frac{1}{\sqrt{2\pi}} \int_{\mathbb{R}} \Psi(x) e^{i\omega x} dx,$$

for continuous Fourier transform, and $A \in \mathbb{Z}_{>0}$ is a scaling parameter that can be arbitrarily chosen. Though with perfect frequency localization, these atoms have slow spatial decay.

A smooth frequency windowing is needed for Gabor atoms with better spatial localization. For this purpose, we can define a bump function

(1.2)
$$g(s) = \begin{cases} \cos(\frac{\pi}{2}\beta(s/\pi)) & \text{if } -\pi < s < \pi, \\ 0 & \text{otherwise,} \end{cases}$$

where the function $\beta(s)$ should satisfy

(1.3)
$$\beta(s) + \beta(1-s) = 1 \text{ and } \beta(-s) = \beta(s).$$

The bump function g(s) can be viewed as a smoothed version of the characteristic function $\chi_{[-\frac{\pi}{2},\frac{\pi}{2}]}$, and the order of smoothness is determined by β . The Gabor atoms with blended frequency windows are given by

$$(1.4) \ \widehat{\psi_{j,p}}(\omega) = \sqrt{\frac{A}{2\pi}} e^{iA\omega p} \left(e^{-i\frac{1}{2}(A\omega - (j+\frac{1}{2})\pi)} g \left(A\omega - (j+\frac{1}{2})\pi \right) + e^{-i\frac{1}{2}(A\omega + (j+\frac{1}{2})\pi)} g \left(A\omega + (j+\frac{1}{2})\pi \right) \right).$$

1.2.2. Wavelets. For wavelets, the phase-space tiling is given as in Figure 1b. More specifically, a wavelet basis is given by a function $\psi : \mathbb{R} \to \mathbb{C}$ and its multiscale counterparts:

$$\psi_{j,p}(x) = \frac{1}{\sqrt{2^j}} \psi\left(\frac{x - 2^j p}{2^j}\right),\,$$

such that $\{\psi_{j,p}\}_{(j,p)\in\mathbb{Z}^2}$ form an orthonormal basis of $L^2(\mathbb{R})$. As a result, their Fourier transforms

(1.5)
$$\widehat{\psi_{j,p}}(\omega) = \sqrt{\frac{2^j}{2\pi}} e^{i2^j \omega p} \widehat{\psi}(2^j \omega)$$

also form an orthonormal basis of $L^2(\mathbb{R})$. When the frequency window $\hat{\psi}(\omega)$ is a sharp indicator function

(1.6)
$$\hat{\psi}(\omega) = \chi_{[-2\pi, -\pi] \cup [\pi, 2\pi]}(\omega) = \chi_{[\pi, 2\pi]}(|\omega|),$$

the resulting basis functions are the Shannon wavelets.

We may also consider smooth blended frequency windows, for example,

$$\hat{\psi}(\omega) = \begin{cases}
e^{-i\frac{\omega}{2}}g\left(\frac{3\omega}{2} - 2\pi\right) & \text{if } \frac{2\pi}{3} \leq \omega \leq \frac{4\pi}{3}, \\
e^{-i\frac{\omega}{2}}g\left(\frac{3\omega}{4} - \pi\right) & \text{if } \frac{4\pi}{3} \leq \omega \leq \frac{8\pi}{3}, \\
0 & \text{if } 0 \leq \omega \leq \frac{2\pi}{3} \text{ or } \omega \geq \frac{8\pi}{3}, \\
\hat{\psi}(-\omega)^* & \text{if } \omega < 0,
\end{cases}$$

where $\hat{\psi}(-\omega)^*$ means the conjugate of complex number $\hat{\psi}(-\omega)$. This results in the famous Meyer wavelets [Mal99, Chapter 7.2.2].

1.3. Notations and conventions. Let us first summarize the notations and conventions used in this paper, which are compatible with the standard notations in quantum computing literature. We use \otimes to denote the tensor product and \oplus for the direct product of matrices. Occasionally, \oplus is also used as the notation of modulo 2 plus in bit-wise operations, but the meaning should be clear based on the context. The notation [M] stands for the set $\{0, 1, \ldots, M-1\}$. The matrix I_M means the identity matrix of dimension M. We use z^* to represent the conjugate of a complex number z, and A^{\dagger} the conjugate transpose of matrix A.

We adopt Dirac's notation $|\cdot\rangle$ to represent a quantum state as a column vector and $\langle \cdot |$ as its conjugate transpose. A qubit lives in the space $\mathbb{C}^2 = \text{span}\{|0\rangle, |1\rangle\}$, where $|0\rangle$ and $|1\rangle$ represent $[1,0]^T$ and $[0,1]^T$, respectively. For a non-negative integer x with binary representation $x = (x_{m-1}x_{m-2} \cdots x_0)_2$, we denote the m-qubit state

$$(1.8) |x\rangle := |x_{m-1}x_{m-2}\cdots x_0\rangle = |x_{m-1}\rangle |x_{m-2}\rangle \cdots |x_0\rangle = |x_{m-1}\rangle \otimes |x_{m-2}\rangle \otimes \cdots \otimes |x_0\rangle.$$

In this convention, we can identify any unit vector $f \in \mathbb{C}^M$ as an m-qubit state $\sum_{x=0}^{M-1} f(x) |x\rangle$. Due to the basic assumptions of quantum mechanics, we always assume the vectors have norm 1, and all operators we consider are unitary matrices correspondingly.

The unitary manipulations are often drawn as boxes in the quantum circuits, where we use horizontal wires to represent qubits. The ordering convention we are using here is the higher digit of the binary representation (1.8) will correspond to the upper qubit when drawing the quantum circuit. More examples of quantum circuits can be found in quantum computing textbooks [Lin22a, NC00]. In the present paper, we denote $n = \log_2 N$ as the number of qubits utilized for implementing the wave packet transform in the space \mathbb{C}^N . Additionally, $M = 2^m$ is often used for the dimension of matrices acting as intermediate steps, with the value of M left temporarily unspecified.

X, Y, Z, and H represent the Pauli-X, Pauli-Y, Pauli-Z, and Hadamard matrices respectively, defined as

$$X = \begin{bmatrix} 0 & 1 \\ 1 & 0 \end{bmatrix}, \qquad \qquad Y = \begin{bmatrix} 0 & -i \\ i & 0 \end{bmatrix}, \qquad \qquad Z = \begin{bmatrix} 1 & 0 \\ 0 & -1 \end{bmatrix}, \qquad \qquad H = \frac{1}{\sqrt{2}} \begin{bmatrix} 1 & 1 \\ 1 & -1 \end{bmatrix}.$$

We also extensively use some basic two-qubit gates. The $|1\rangle$ -controlled-NOT gate is $|0\rangle\langle 0| \otimes I_2 + |1\rangle\langle 1| \otimes X$, and is usually just called the CNOT gate. In a quantum circuit, this gate is drawn as in Figure 2a, where the filled node means only applying the lower gate when the upper qubit is $|1\rangle$. We usually use " \oplus " to represent "X" in quantum circuits. The related $|0\rangle$ -controlled-NOT gate, $|0\rangle\langle 0| \otimes X + |1\rangle\langle 1| \otimes I_2$, is given in Figure 2b, where the unfilled node has just the opposite meaning as the filled one. The swap gate SWAP = $|00\rangle\langle 00| + |01\rangle\langle 10| + |10\rangle\langle 01| + |11\rangle\langle 11|$, which swaps the value of two qubits, is shown as Figure 2c. We sometimes also make use of the multi-qubit controlled gate, which can be built by single qubit gates and CNOT gates [BBC+95]. For instance, $|11\rangle\langle 11| \otimes U + (I_4 - |11\rangle\langle 11|) \otimes I$ is shown in Figure 2d.

Figure 2. (a) CNOT gate. (b) $|0\rangle$ -controlled-NOT gate. (c) SWAP gate. (d) An example of a multi-qubit control gate $|11\rangle\langle11|\otimes U+(I_4-|11\rangle\langle11|)\otimes I$. The two filled nodes indicate that U is applied to the third qubit if and only if both the first two qubits are at state $|1\rangle$.

An (m+n)-qubit unitary operator U is called a (γ, m, ϵ) -block-encoding of an $N \times N$ matrix A, if

$$||A - \gamma(\langle 0^m | \otimes I_N) U(|0^m \rangle \otimes I_N)|| \le \epsilon.$$

In the matrix form, a (γ, m, ϵ) -block-encoding is a 2^{m+n} dimensional unitary matrix

$$U = \left(\begin{array}{cc} \widetilde{A}/\gamma & * \\ * & * \end{array}\right)$$

where * can be any block matrices of the correct size, and $\|\widetilde{A} - A\| \le \epsilon$.

The inner product of two complex vectors f_1 and f_2 is denoted by

(1.9)
$$\langle f_1 | f_2 \rangle := \langle f_1, f_2 \rangle = \sum_{t=0}^{N-1} f_1(t) f_2(t)^*.$$

We denote $f(m_1:m_2)$ as the restriction of vector f from the m_1 -th element to the m_2 -th element.

For any j in the computational basis, the (discrete) forward Fourier transform is defined as

$$U_{\mathrm{FT}(N)}|j\rangle = \frac{1}{\sqrt{N}} \sum_{k \in [N]} \mathrm{e}^{\mathrm{i}2\pi \frac{kj}{N}} |k\rangle,$$

which is widely used in the quantum computing literature but has a sign difference compared to the classical signal processing convention.

The indices of vectors in this paper are always considered in the modulo N sense, i.e., f(-k) = f(N-k). In particular, we adopt the convention $|-k\rangle = |N-k\rangle$ in the bracket notation.

For all matrices, the subscripts "G" and "W" indicate that they are related to Gabor atoms and wavelets, respectively. The subscripts "S" and "B" stand for sharp and blended frequency windows, respectively. In particular, the four main transformations in the paper are denoted as $U_{\rm GS}$, $U_{\rm GB}$, $U_{\rm WS}$, and $U_{\rm WB}$, i.e., sharp Gabor atoms, blended Gabor atoms, Shannon (sharp) wavelets, and Meyer (blended) wavelets. For the matrices that we want to specify the dimension, we write the dimension as a subscript. The italicized subscripts representing dimensions, such as N, M, and B, can be readily distinguished from the Roman subscripts denoting names, such as the aforementioned "G", "W", "S", and "B".

2. Gabor atoms

This section delves into the implementation of the quantum version of the Gabor atom transform. Specifically, we will discuss the discretization and present the quantum circuits for both the sharp Gabor atoms (1.1) and the blended Gabor atoms (1.4). Implementing the sharp Gabor atoms can be viewed as first reshuffling the Fourier transform \hat{f} of the input and then performing an inverse Fourier transform for each sharp frequency window. The blended Gabor atoms are more intricate due to the overlapping of neighboring packets. Our approach entails first recombining parts of \hat{f} to the proper locations, which is a unitary process, and then applying the circuit of the sharp Gabor atoms. The recombining process involves the implementation of certain diagonal matrices, which will also be discussed in detail.

2.1. Sharp Gabor atoms. Given the basis functions (1.1), let us introduce the discrete sharp Gabor atoms in the frequency domain. We restrict $\omega \in [-\pi, \pi)$ to grid points $\{\frac{2\pi}{N}k\}$, where $k = -N/2, \ldots, N/2-1$. Denote $B = \frac{N}{2A}$ and $b = \log_2 B$. The discrete sharp Gabor atoms are defined in the (discrete) frequency space as

$$\widehat{\psi_{j,p}}(k) := \frac{1}{\sqrt{2B}} e^{2\pi i \frac{pk}{2B}} \left[\chi_{[jB,(j+1)B)}(k) + \chi_{[-(j+1)B,-jB)}(k) \right],$$

where $\psi_{j,p}$ is for the discrete basis function in order to distinguish from its continuous counterpart $\psi_{j,p}$. We also point out that the discrete and continuous basis corresponds in the sense that $\widehat{\psi_{j,p}}(k) := \sqrt{\frac{2\pi}{N}}\widehat{\psi_{j,p}}(\frac{2\pi}{N}k)$. Only the basis function with indices $j \in [A]$ and $p \in [2B]$ are used in the discrete setting, which is in total N basis functions. Typically, we may choose $A = 2^{\lfloor n/2 \rfloor}$ and $B = 2^{\lfloor (n-1)/2 \rfloor}$ to balance the resolution of space and frequency, though other choices of A and B are also acceptable. To simplify indexing, we further denote $\psi_{j,p}$ as ψ_{2Bj+p} , thereby aligning the basis functions with indices ranging from 0 to N-1. More explicitly, the Fourier coefficients of the sharp Gabor atoms basis are

(2.1)
$$\widehat{\psi_{2Bj+p}}(k) := \widehat{\psi_{j,p}}(k),$$

for $j \in [\frac{N}{2B}]$, $p \in [2B]$, and $k \in \{-\frac{N}{2}, -\frac{N}{2} + 1, \dots, \frac{N}{2} - 1\}$. Here, χ_I means the characteristic function on interval I. In some other literature, there may be an additional phase on the characteristic functions in the sharp Gabor atoms, which is not adopted here and can be viewed as a special version of the blended Gabor atoms discussed in Section 2.2.

For a signal $f \in \mathbb{C}^N$, one can expand f under this basis

(2.2)
$$f = \sum_{j \in [\frac{N}{2D}]} \sum_{p \in [2B]} a_{2Bj+p} \psi_{2Bj+p} = \sum_{n=0}^{N-1} a_n \psi_n,$$

where a_{2Bj+p} 's are the Gabor atom coefficients. Notice that the ψ_{2Bj+p} here is the discrete Fourier inverse of (2.1), which is not the direct restriction of the continuous $\psi_{j,p}$ in the space domain. The sharp Gabor atom transform is defined as

$$(2.3) U_{GS}: \mathbb{C}^N \to \mathbb{C}^N: f \mapsto a = (a_0, a_1, \dots, a_{N-1})^T.$$

One can check that the basis given by (2.1) is orthonormal. Therefore, the coefficients of signal f are given by the inner product

$$(2.4) a_{2Bj+p} = \langle f, \psi_{2Bj+p} \rangle = \langle \hat{f}, \widehat{\psi_{2Bj+p}} \rangle = \left(\sum_{k=jB}^{(j+1)B-1} + \sum_{k=-(j+1)B}^{-jB-1} \right) \frac{1}{\sqrt{2B}} e^{-2\pi i \frac{pk}{2B}} \hat{f}(k),$$

where the second step is the Plancherel's identity. When j is even, this gives

$$(2.5) a_{2Bj+p} = \frac{1}{\sqrt{2B}} \left(\sum_{k=0}^{B-1} e^{-2\pi i \frac{p(k+jB)}{2B}} \hat{f}(k+jB) + \sum_{k=B}^{2B-1} e^{-2\pi i \frac{p(k-(j+2)B)}{2B}} \hat{f}(k-(j+2)B) \right)$$

$$= \frac{1}{\sqrt{2B}} \left(\sum_{k=0}^{B-1} e^{-2\pi i \frac{pk}{2B}} \hat{f}(k+jB) + \sum_{k=B}^{2B-1} e^{-2\pi i \frac{pk}{2B}} \hat{f}(k-(j+2)B) \right).$$

Similarly, when j is odd,

$$(2.6) a_{2Bj+p} = \frac{1}{\sqrt{2B}} \left(\sum_{k=0}^{B-1} e^{-2\pi i \frac{pk}{2B}} \hat{f}(k - (j+1)B) + \sum_{k=B}^{2B-1} e^{-2\pi i \frac{pk}{2B}} \hat{f}(k + (j-1)B) \right).$$

This form implies that if we permute the elements of \hat{f} , then a_{2Bj+p} can be obtained from an inverse Fourier transform of size 2B. Specifically, let $S_{G(N,B)}$ be the permutation matrix such that for $j \in [\frac{N}{2B}]$, $k \in [B]$, we have

$$(2.7)$$

$$S_{G(N,B)} |Bj+k\rangle = \begin{cases} |2Bj+k\rangle & \text{if } j \text{ is even,} \\ |2Bj+B+k\rangle & \text{if } j \text{ is odd,} \end{cases}$$

$$S_{G(N,B)} |B(\frac{N}{B}-1-j)+k\rangle = \begin{cases} |2Bj+k\rangle & \text{if } j \text{ is odd,} \\ |2Bj+B+k\rangle & \text{if } j \text{ is even.} \end{cases}$$

After acting $S_{G(N,B)}$ on \hat{f} , we have

(2.8)
$$a_{2Bj+p} = \frac{1}{\sqrt{2B}} \left(\sum_{k=0}^{2B-1} e^{-2\pi i \frac{pk}{2B}} (S_{G(N,B)} \hat{f})(k+2Bj) \right),$$

which is just an inverse Fourier transform of size 2B as desired. This process is shown in Figure 3.

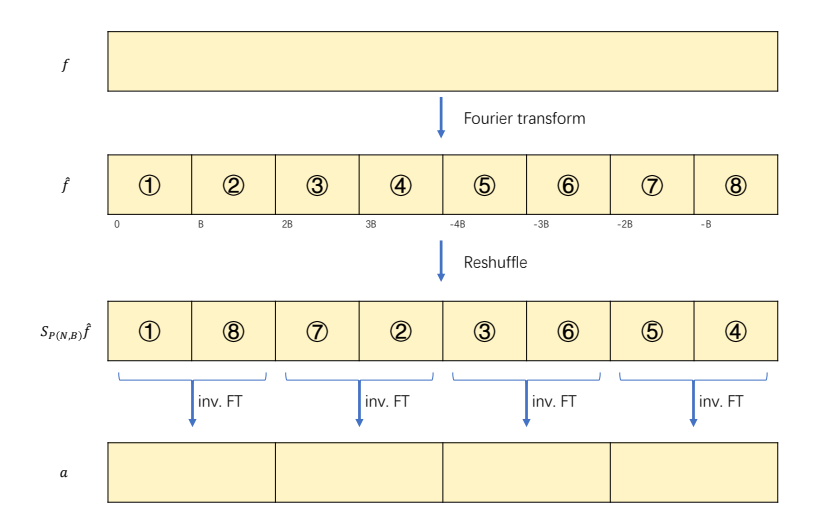


Figure 3. The process of sharp Gabor atoms transform. Reshuffle the indices in the frequency domain, and then perform an inverse Fourier transform on each of the 2B-size blocks.

As an intermediate step of the implementation of $S_{G(N,B)}$, we first introduce another permutation matrix. For an integer m and $M = 2^m$, let $G_{G(M)}$ be the $M \times M$ permutation matrix such that

(2.9)
$$G_{G(M)} |j\rangle = |2j\rangle,$$

$$G_{G(M)} |M - 1 - j\rangle = |2j + 1\rangle,$$

for $j \in [M/2]$. Notice that $G_{\mathrm{G}(M)}$ can be represented by the bit manipulation

$$(2.10) |x_{m-1}x_{m-2}\cdots x_0\rangle \mapsto |x_{m-1}(x_{m-2}\oplus x_{m-1})\cdots (x_0\oplus x_{m-1})\rangle \mapsto |(x_{m-2}\oplus x_{m-1})\cdots (x_0\oplus x_{m-1})x_{m-1}\rangle,$$

therefore it can be implemented on the quantum computer by m-1 CNOT-gates followed by m-1 SWAP-gates.

Now let us come back to the implementation of matrix $S_{G(N,B)}$. One can see that $S_{G(N,B)}$ only operates on the first n-b qubits, and can be factorized as

$$S_{\mathrm{G}(N,B)} = S_{\mathrm{G}(\frac{N}{D},1)} \otimes I_{2^b} = (I_{2^{n-b-2}} \otimes \mathrm{CNOT} \otimes I_{2^b})(G_{\mathrm{G}(N/B)} \otimes I_{2^b}).$$

Here, the extra CNOT-gate is used for deciding whether the j in (2.7) is even or odd. If j is odd, we need an extra switch between $|2Bj + k\rangle$ and $|2Bj + B + k\rangle$ after applying $G_{G(N/B)}$ on the first n - b qubits.

Finally, the complete circuit from f to a is given by

$$(2.11) U_{GS} = (I_{2^{n-b-1}} \otimes U_{FT(2B)}^{\dagger})(I_{2^{n-b-2}} \otimes CNOT \otimes I_{2^b})(G_{G(N/B)} \otimes I_{2^b})U_{FT(N)},$$

which is demonstrated in Figure 4.

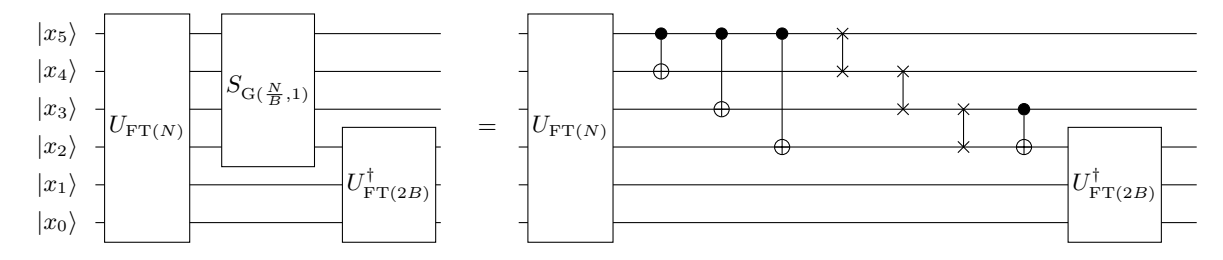


Figure 4. The circuit of U_{GS} when N=64 and B=4.

2.2. **Blended Gabor atoms.** As discussed in Section 1.2, the aim of introducing the blended Gabor atoms is to incorporate blended frequency windows, resulting in rapid decay in the space domain. Typically, a blended Gabor atom basis function consists of two frequency bumps symmetrically positioned about the origin, such as the second and seventh bump in Figure 5.

To define the discrete blended Gabor atoms, we restrict ω onto a grid and represent the index (j, p) as 2Bj + p for convenience in ordering. The Fourier transform of a discrete blended Gabor atom is defined by (2.12)

$$\widehat{\psi_{2Bj+p}}(k) = \frac{1}{\sqrt{2B}} e^{2\pi i \frac{pk}{2B}} \left[e^{\frac{1}{2}\pi i \left(\frac{1}{2} - \frac{k-Bj}{B}\right)} g_{\text{per}} \left(\pi \left(\frac{k-Bj}{B} - \frac{1}{2} \right) \right) + e^{\frac{1}{2}\pi i \left(-\frac{1}{2} - \frac{k+Bj}{B} \right)} g_{\text{per}} \left(\pi \left(\frac{k+Bj}{B} + \frac{1}{2} \right) \right) \right]$$

for $j \in \left[\frac{N}{2B}\right]$, $p \in [2B]$, where

(2.13)
$$g_{\text{per}}(x) = \sum_{q \in \mathbb{Z}} g(x + q\pi \frac{N}{B})$$

is the periodic version of g defined in (1.2). Here, g_{per} is used instead of g due to the considerations of boundary conditions. This periodization also automatically makes $\widehat{\psi_{2Bj+p}}(k) = \widehat{\psi_{2Bj+p}}(N+k)$ hold for any integer k, which is compatible with our convention.

We also point out that, akin to the sharp Gabor atom, this discrete basis function corresponds to its continuous counterpart through $\widehat{\psi_{j,p}}(\frac{2\pi}{N}k) = \sqrt{\frac{2\pi}{N}}\widehat{\psi_{j,p}}(k)$, except for those k values near the boundary.

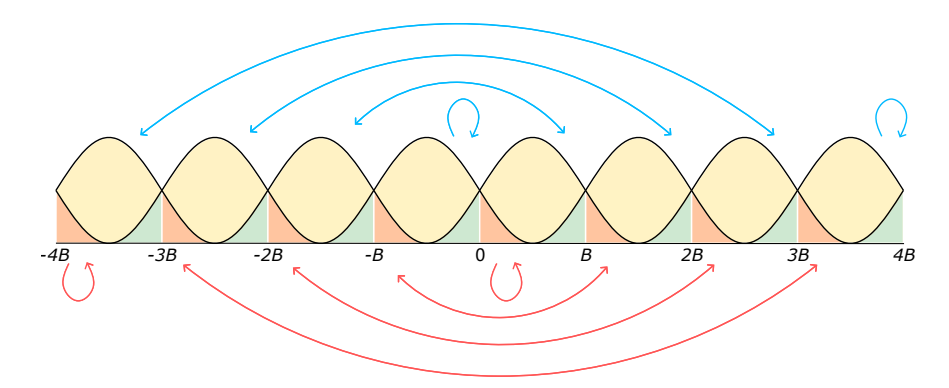


Figure 5. Illustration of reallocation when N=8B. Each basis function $\widehat{\psi_{2Bj+p}}$ contains two bumps supported at $[(j-\frac{1}{2})B,(j+\frac{3}{2})B)$ and $[-(j+\frac{3}{2})B,-(j-\frac{1}{2})B)$. The arrows indicate how the small tails are transposed such that all the relevant $\widehat{f}(k)$'s are placed in $[jB,(j+1)B) \cup [-(j+1)B,-jB)$ with correct proportion. All these reallocations are unitary manipulations. This figure exclusively illustrates magnitude transpositions, omitting the change of phase. In particular, the self-transpositions are, in fact, phase rotations.

One can make straightforward calculations to show that $\psi_0, \ldots, \psi_{N-1}$ form an orthonormal basis of \mathbb{C}^N . Similar to the sharp case, the coefficients of a vector f are $a_{2Bj+p} = \langle \hat{f}, \widehat{\psi_{2Bj+p}} \rangle$, and the blended Gabor atom transform is defined as

(2.14)
$$U_{GB}: \mathbb{C}^N \to \mathbb{C}^N: f \mapsto a = (a_0, a_1, \dots, a_{N-1})^T.$$

In this scenario, the support of different basis functions may intersect. Therefore, we first reallocate \hat{f} to the correct position. Subsequently, we perform the rearrangement of indices, identical to the procedure for sharp Gabor atoms. This reallocation process is shown in Figure 5. To make it mathematically concrete, we introduce the intermediate variable h(k) defined as

$$(2.15) \qquad \qquad h(jB+q) = \hat{f}(jB+q)g\left(-\frac{\pi}{2} + q\frac{\pi}{B}\right)e^{\frac{i}{2}(-\frac{\pi}{2} + q\frac{\pi}{B})} + \hat{f}(-jB+q)g\left(\frac{\pi}{2} + q\frac{\pi}{B}\right)e^{\frac{i}{2}(\frac{\pi}{2} + q\frac{\pi}{B})},$$

$$(2.16) \quad h((j+\frac{1}{2})B+q) = \hat{f}((j+\frac{1}{2})B+q)g\left(q\frac{\pi}{B}\right)e^{\frac{i}{2}(q\frac{\pi}{B})} + \hat{f}(-(j+\frac{3}{2})B+q)g\left(-\pi+q\frac{\pi}{B}\right)e^{\frac{i}{2}(-\pi+q\frac{\pi}{B})}$$

for $j=-\frac{N}{2B},-\frac{N}{2B}+1,\ldots,\frac{N}{2B}-1,\,q\in[\frac{B}{2}].$ This reallocation process guarantees that

(2.17)
$$\left(\sum_{k=jB}^{(j+1)B-1} + \sum_{k=-(j+1)B}^{-jB-1}\right) \frac{1}{\sqrt{2B}} e^{-2\pi i \frac{pk}{2B}} h(k) = \langle \hat{f}, \widehat{\psi_{2Bj+p}} \rangle = a_{2Bj+p}.$$

The proof is provided in Section 4.1. Despite its complex appearance, the formulas for h(k) are derived in reverse to satisfy (2.17), so the proof is straightforward calculations.

Notice that (2.17) and (2.4) share the same form, so we can reuse the circuit in Section 2.1, and conclude that the complete circuit from blended Gabor atom transform $U_{GB}: f \mapsto a$ is given by

(2.18)
$$U_{GB} = (I_{2^{n-b-1}} \otimes U_{FT(2B)}^{\dagger}) S_{G(N,B)} T_G U_{FT(N)},$$

where $T_{\rm G}$ is the transition matrix from \hat{f} to h, and can be written down following the definitions in (2.15) and (2.16).

Let us now focus on the implementation of T_G . Since T_G has the potential block-diagonal structure, as shown in Figure 6a, we shall first rearrange the order of the computational basis to reveal this structure. At this stage, we do not need to deal with the last b-1 qubits. For an integer $M=2^m$, we may define the

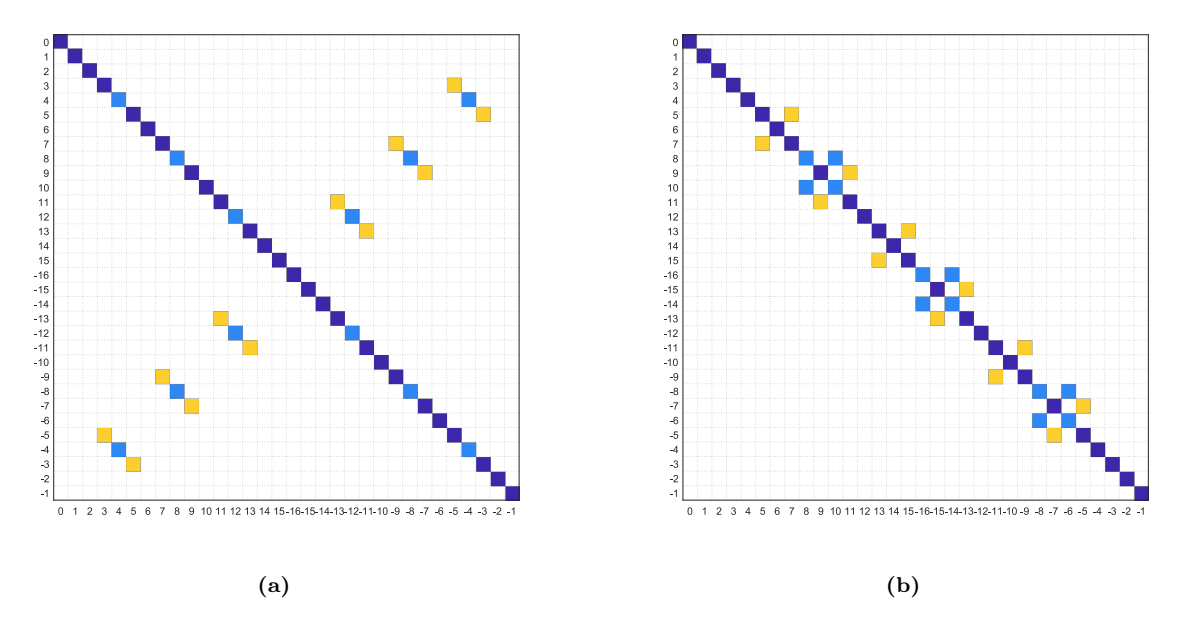


Figure 6. (a) Magnitude of elements in $T_{\rm G}$ with $N=32,\,B=4$. (b) Magnitude of elements in $V_{\rm G}$ with $N=32,\,B=4$.

permutation matrix $Q_{G(M)}$ as

$$Q_{G(M)} | j \rangle = | 2j \rangle, \quad \text{for } j \in [M/2],$$

$$Q_{G(M)} | M - 1 \rangle = | M - 1 \rangle,$$

$$Q_{G(M)} | M/2 \rangle = | 1 \rangle,$$

$$Q_{G(M)} | M - 2j \rangle = | 4j + 1 \rangle, \quad \text{for } j = 1, 2, \dots, M/4 - 1,$$

$$Q_{G(M)} | M - 2j - 1 \rangle = | 4j - 1 \rangle, \quad \text{for } j = 1, 2, \dots, M/4 - 1.$$

The detailed implementation of $Q_{\mathrm{G}(M)}$ is shown in Section 2.2.1. We can use the permutation matrix $Q_{\mathrm{G}(\frac{2N}{B})} \otimes I_{2^{b-1}}$ to rearrange the nonzero elements in T_{G} and define a new matrix

(2.20)
$$V_{G} = (Q_{G(\frac{2N}{B})} \otimes I_{2^{b-1}})^{\dagger} T_{G}(Q_{G(\frac{2N}{B})} \otimes I_{2^{b-1}}),$$

which is a block-diagonal matrix as shown in Figure 6b. A detailed description of $V_{\rm G}$ and its implementation is discussed in Section 2.2.2. Combining (2.18) and (2.20), we can draw the complete circuit of $U_{\rm GB}$ in Figure 7.

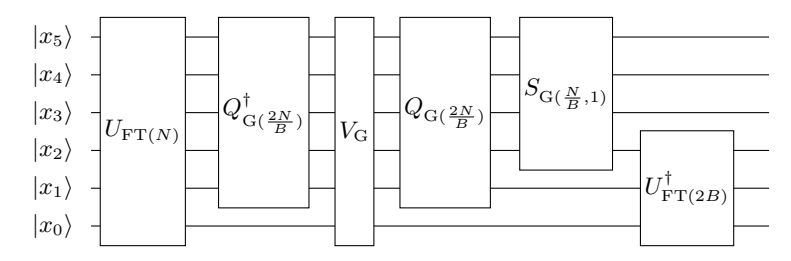


Figure 7. The circuit of U_{GB} when N=64 and B=4.

2.2.1. The implementation of $Q_{G(M)}$. Let L be the $M \times M$ shift matrix

(2.21)
$$L = \begin{bmatrix} 0 & 0 & \dots & 1 \\ 1 & 0 & 0 & \ddots & 0 \\ \vdots & 1 & \ddots & \ddots & \vdots \\ \vdots & \ddots & \ddots & \ddots & \vdots \\ 0 & 0 & \dots & 1 & 0 \end{bmatrix},$$

which can be implemented easily within $O(m^2)$ gate complexity, as shown in [CLVBY22, Figure 6]. If one is allowed to use one ancilla qubit, then L can be implemented within O(m) gate complexity as in [Kla99].

Notice that $Q_{\mathcal{G}(M)}$ has the same M/2 columns as the matrix $G_{\mathcal{G}(M)}$ introduced earlier, so it is natural to reuse the circuit of $G_{\mathcal{G}(M)}$ in the construction of $Q_{\mathcal{G}(M)}$. Straightforward calculations show that $G_{\mathcal{G}(M)}^{-1}Q_{\mathcal{G}(M)}$ is a permutation matrix that switches $|M-2j\rangle$ and $|M-2j-1\rangle$ for $j=1,2,\ldots,\frac{M}{4}-1$, and also switches $|M-1\rangle$ and $|M/2\rangle$. Therefore, we have $G_{\mathcal{G}(M)}^{-1}Q_{\mathcal{G}(M)}=|0\rangle\langle 0|\otimes I_{M/2}+|1\rangle\langle 1|\otimes (L(I_{M/4}\otimes X)L^{\dagger})$. Finally, noticing that the controls on L and L^{\dagger} are unnecessary since they will be canceled, we conclude

$$(2.22) Q_{G(M)} = G_{G(M)}(I_2 \otimes L) \left(|0\rangle\langle 0| \otimes I_{M/2} + |1\rangle\langle 1| \otimes I_{M/4} \otimes X \right) (I_2 \otimes L)^{\dagger},$$

where $(|0\rangle\langle 0| \otimes I_{M/2} + |1\rangle\langle 1| \otimes I_{M/4} \otimes X)$ is just the CNOT gate on the first and the last qubits. Figure 8 illustrates the circuit implementation of $Q_{G(M)}$.

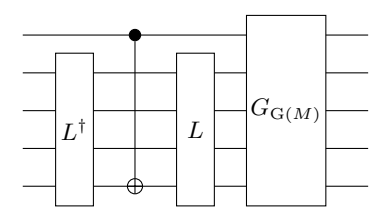


Figure 8. The circuit of $Q_{G(M)}$ for M=32.

2.2.2. Implementation of V_G . To help the following discussion, we define two diagonal matrices $D_+ = \text{diag}\{0,\frac{1}{B},\frac{2}{B},\dots,\frac{(B/2-1)}{B}\}$ and $D_- = D_+ - \frac{1}{2}I$.

As illustrated in Figure 6b, the matrix V_G is a block-diagonal matrix with $\frac{N}{B}$ blocks, with each block of size $B \times B$. By the definitions in (2.15) and (2.16) together with the permutation matrix $Q_{G(M)}$, we can write down the blocks explicitly.

The 0-th block =
$$\hat{K}_e := I_2 \otimes e^{\frac{i}{2}(\pi\beta(D_-)+\pi D_-)}$$
.
The $(2j)$ -th block = $K_e := \begin{bmatrix} \cos(\frac{\pi}{2}\beta(D_-))e^{\frac{i}{2}\pi D_-} & i\sin(\frac{\pi}{2}\beta(D_-))e^{\frac{i}{2}\pi D_-} \\ i\sin(\frac{\pi}{2}\beta(D_-))e^{\frac{i}{2}\pi D_-} & \cos(\frac{\pi}{2}\beta(D_-))e^{\frac{i}{2}\pi D_-} \end{bmatrix}$
= $(H \otimes I_{B/2}) \begin{bmatrix} e^{\frac{i}{2}(\pi\beta(D_-)+\pi D_-)} & 0 \\ 0 & e^{\frac{i}{2}(-\pi\beta(D_-)+\pi D_-)} \end{bmatrix} (H \otimes I_{B/2}),$
for $j = 1, 2, ..., \frac{N}{2B} - 1$.
(2.23)

The $(2j-1)$ -th block = $K_o := \begin{bmatrix} \cos(\frac{\pi}{2}\beta(D_+))e^{\frac{i}{2}\pi D_+} & -i\sin(\frac{\pi}{2}\beta(D_+))e^{\frac{i}{2}\pi D_+} \\ -i\sin(\frac{\pi}{2}\beta(D_+))e^{\frac{i}{2}\pi D_+} & \cos(\frac{\pi}{2}\beta(D_+))e^{\frac{i}{2}\pi D_+} \end{bmatrix}$
= $(H \otimes I_{B/2}) \begin{bmatrix} e^{\frac{i}{2}(-\pi\beta(D_+)+\pi D_+)} & 0 \\ 0 & e^{\frac{i}{2}(\pi\beta(D_+)+\pi D_+)} \end{bmatrix} (H \otimes I_{B/2}),$
for $j = 1, 2, ..., \frac{N}{2B} - 1$.
The $(\frac{N}{B} - 1)$ -th block = $\hat{K}_o := I_2 \otimes e^{\frac{i}{2}(-\pi\beta(D_+)+\pi D_+)}.$

The remaining challenge lies in implementing these diagonal matrices. Usually, $\beta(x)$ will be chosen as a polynomial on $[0, \frac{1}{2}]$ and then extend to [-1, 1] according to (1.3). Typical choices include $\beta(x) = x$ or $\beta(x) = 2x^2$ in the interval $[0, \frac{1}{2}]$. For such low-degree β , one can use the method introduced in Section 2.2.3 to implement the required diagonal matrices. If one wants to pursue higher regularity with more sophisticated $\beta(x)$, such as

$$\beta(x) = x^4(35 - 84x + 70x^2 - 20x^3), \quad \text{for } x \in [0, 1],$$

or even non-polynomial functions, the method in Section 2.2.4 could be used.

Finally, the circuit of $V_{\rm G}$ is presented in Figure 9. Here, we need to implement the multi-qubit controlled version of a unitary. A naive way is to do the multi-qubit controlled version of every gate in this unitary in order. However, this approach results in very high gate complexity. Instead, we may introduce an ancilla qubit to make the implementation using mainly single qubit controls, as demonstrated in Figure 10.

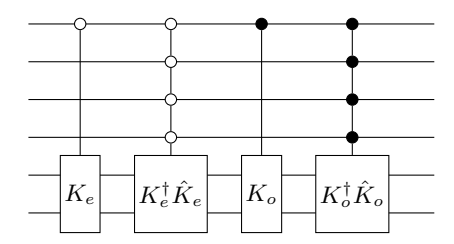


Figure 9. The circuit of V_G when N = 64 and B = 4.

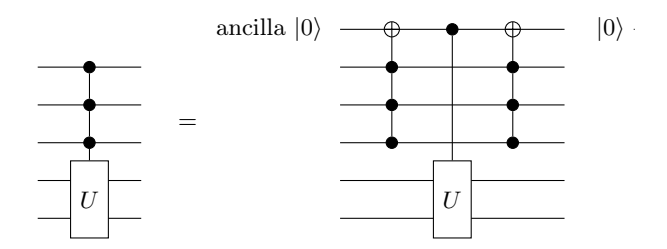


Figure 10. The circuit of implementing multi-qubit controlled unitaries using one ancilla qubit.

2.2.3. Implementation of the exponential of a pure imaginary polynomial via bit manipulations. Now we focus on the general problem of implementing diagonal matrices $\exp(iq(A))$, where $A = \operatorname{diag}\{0,1,\ldots,M-1\}$ for some $M=2^m$, and q is a real polynomial. Since polynomials are the sum of monomials, we only need to consider the special case $q(A)=rA^s$, where $r\in\mathbb{R}$ and $s\geq 0$ is integer. The case s=0 is trivial. The case s=1 is discussed in [LNY23, Section 5.1], which exploits the following observation. Let $x\in[M]$ and $x=(x_{m-1}\cdots x_0)_2$ be its binary representation, then

$$(2.25) \qquad \exp(irA) |x\rangle = \exp(irx) |x\rangle = \bigotimes_{j=0}^{m-1} \left(\exp(irx_j 2^j) |x_j\rangle \right) = \bigotimes_{j=0}^{m-1} \left(R_z(2^j r) |x_j\rangle \right).$$

Where $R_z(\theta) := \begin{pmatrix} 1 \\ e^{i\theta} \end{pmatrix}$ is the single-qubit rotation gate. This means $\exp(irA)$ can be implemented by simply applying an $R_z(2^j r)$ on the j-th qubit.

For general s, a similar approach can be utilized, but it may involve multi-qubit gates due to the cross terms. Specifically, we have

$$(2.26) x^{s} = \left(\sum_{j=0}^{m-1} 2^{j} x_{j}\right)^{s} = \sum_{k_{0} + k_{1} + \dots + k_{m-1} = s; k_{j} \ge 0} {n \choose k_{0}, k_{1}, \dots, k_{m-1}} \prod_{j=0}^{m-1} (2^{jk_{j}} x_{j}^{k_{j}})$$

$$= \sum_{k_{0} + k_{1} + \dots + k_{m-1} = s; k_{j} \ge 0} {n \choose k_{0}, k_{1}, \dots, k_{m-1}} \left(\prod_{j=0}^{m-1} 2^{jk_{j}}\right) \prod_{k_{j} > 0} x_{j}.$$

Therefore, to implement $\exp(icx^s)$, we only need to implement the terms look like $\exp(ic\prod_{j\in J}x_j)$, where J is an index set, and c is a real number. This $2^{|J|}$ dimensional matrix can be realized as a controlled version of $R_z(c)$, which is

(2.27)
$$\operatorname{diag}\{1,1,\ldots,1,e^{ic}\} = |1^{|J|-1}\rangle\langle 1^{|J|-1}| \otimes R_z(c) + (I-|1^{|J|-1})\langle 1^{|J|-1}|) \otimes I.$$

Note that it does not matter which |J| - 1 qubits serve as control qubits since this matrix will not change under different choices.

To demonstrate this clearly, we give an example for m = 3, s = 3, r = 1. In this case,

(2.28)
$$\exp(ix^3)|x\rangle = \exp(i(x_0 + 8x_1 + 64x_2 + 18x_0x_1 + 60x_0x_2 + 144x_1x_2 + 48x_0x_1x_2))|x_2x_1x_0\rangle$$
, which can be implemented as Figure 11.

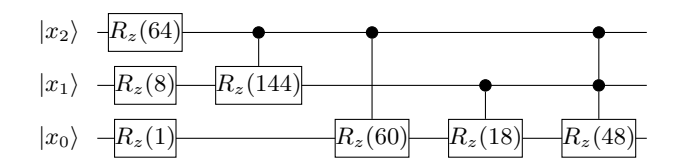


Figure 11. The implementation of the unitary $\sum_{x=0}^{7} \exp(ix^3) |x\rangle\langle x|$.

This method's advantage is that it does not use any ancilla qubit and does not introduce any approximation, so it is desirable as long as we have a moderate value of s.

2.2.4. Implementation of the exponential of a pure imaginary polynomial via QSVT. The complexity of the implementation given in Section 2.2.3 is $O(m^s)$, where m is the number of qubits, and s is the degree of polynomial q. This complexity is unaffordable when the degree s is large.

For polynomial q of higher degrees, one may resort to QSVT [GSLW18] for better asymptotic complexity scaling at the expense of introducing approximations and extra ancilla qubits. To be specific, we shall construct a $(\sqrt{2}, 3, \epsilon)$ -block encoding of the desired unitary matrix using QSVT, where ϵ is the tolerable error, and then use the "perfect amplitude amplification" [BAG23] to extract the desired matrix. (One may refer to Section 1.3 for the terminology regarding block encoding.)

Recall that β is a polynomial on [-1,1] satisfying (1.3), and a typical example is (2.24). Therefore, $\gamma(x) := 2\beta(x + \frac{1}{2}) - 1$ is an odd polynomial. The diagonal matrices that we need to implement in (2.23) are $e^{\frac{i}{2}(\pi\beta(D_-) + \pi D_-)}$, $e^{\frac{i}{2}(-\pi\beta(D_-) + \pi D_-)}$, $e^{\frac{i}{2}(-\pi\beta(D_-) + \pi D_-)}$, and $e^{\frac{i}{2}(\pi\beta(D_+) + \pi D_+)}$.

Now we consider $e^{\frac{i}{2}(\pi\beta(D_-)+\pi D_-)}$ as an example since the implementations for the other three matrices are analogous. In this case, the number of qubits is $m = b - 1 = \log_2 B - 1$. Noticing that

$$e^{\frac{i}{2}\pi(\beta(D_{-})+D_{-})} = e^{\frac{i}{2}\pi(-\beta(-D_{-})+D_{-})} = e^{\frac{i}{2}\pi(-\frac{1}{2}(\gamma(-D_{-}-\frac{1}{2})+1)+D_{-})} = e^{-\frac{i\pi}{4}\gamma(-D_{-}-\frac{1}{2})}e^{-\frac{i\pi}{4}+\frac{i\pi}{2}D_{-}},$$

where $e^{-\frac{i\pi}{4} + \frac{i\pi}{2}D_{-}}$ can be easily implemented using the method in Section 2.2.3, we focus on

$$e^{-\frac{i\pi}{4}\gamma(W)} = \cos(\frac{\pi}{4}\gamma(W)) - i\sin(\frac{\pi}{4}\gamma(W)),$$

where $W := -D_- - \frac{1}{2}$ for the simplicity of notations. We need to first implement the $(1, 2, \epsilon)$ -block encodings of $\cos(\frac{\pi}{4}\gamma(W))$ and $\sin(\frac{\pi}{4}\gamma(W))$, and then use LCU [Lin22b, Section 7.3] to get a $(\sqrt{2}, 3, \epsilon)$ -block encoding of $e^{-\frac{i\pi}{4}\gamma(W)}$. Below, we explain this idea in more detail.

For the $(1,2,\epsilon)$ -block encoding of $\cos(\frac{\pi}{4}\gamma(W))$, we outline the procedure following the methodology detailed in [LNY23, Section 5.1]. First, we can use the method in Section 2.2.3 to construct the (1,1,0)-block encoding of $\sin(W)$, given by

$$\begin{bmatrix} \sin(W) & -i\cos(W) \\ -i\cos(W) & \sin(W) \end{bmatrix} = (H \otimes I) \begin{bmatrix} -iI & 0 \\ & iI \end{bmatrix} \begin{bmatrix} e^{iW} & 0 \\ 0 & e^{-iW} \end{bmatrix} (H \otimes I).$$

As $-\frac{1}{2}I \leq W \leq \frac{1}{2}I$, we seek an ϵ accurate polynomial approximation of the even function $\cos(\frac{\pi}{4}(\gamma(\arcsin(x))))$ for $x \in [-\sin(\frac{1}{2}),\sin(\frac{1}{2})]$ to utilize QSVT on $\sin(W)$ to obtain a $(1,2,\epsilon)$ -block encoding of $\cos(\frac{\pi}{4}(\gamma(W)))$. Let $m_{\gamma} = \max_{-\frac{1}{2} \leq x \leq \frac{1}{2}} |\gamma'(x)|$. By truncating the Taylor series of $\arcsin(x)$ at x = 0 to degree $O(\log(\frac{2m_{\gamma}}{\epsilon}))$, we get a polynomial w(x) satisfying $|w(x) - \arcsin(x)| \leq \frac{\epsilon}{2m_{\gamma}}$ for $|x| \leq \sin(\frac{1}{2})$. Consequently, $|\gamma(w(x)) - \gamma(\arcsin(x))| \leq \frac{\epsilon}{2}$. We can also expand $\cos(\frac{\pi}{4}y)$ as Taylor series at y = 0 and truncate at degree $O(\log\frac{1}{\epsilon})$ to obtain a polynomial r(y) such that $|r(y) - \cos(\frac{\pi}{4}y)| \leq \frac{\epsilon}{2}$ for $|y| \leq 1$. Given that $|\gamma(x)| \leq 1$ for $x \in [-\frac{1}{2}, \frac{1}{2}]$, we finally derive

$$\begin{split} & \left| r(\gamma(w(x))) - \cos(\frac{\pi}{4}(\gamma(\arcsin(x)))) \right| \\ & \leq \left| r(\gamma(w(x))) - \cos(\frac{\pi}{4}\gamma(w(x))) \right| + \left| \cos(\frac{\pi}{4}\gamma(w(x))) - \cos(\frac{\pi}{4}(\gamma(\arcsin(x)))) \right| \\ & \leq \frac{\epsilon}{2} + \frac{\epsilon}{2} \max_{y} \left| \frac{\mathrm{d}\cos(\frac{\pi}{4}y)}{\mathrm{d}y} \right| \leq \epsilon. \end{split}$$

Therefore, this polynomial $r(\gamma(w(x)))$ of degee $O(\log(\frac{1}{\epsilon})\log(\frac{2m_{\gamma}}{\epsilon})\deg(\gamma))$ is an ϵ accurate polynomial approximation of the even function $\cos(\frac{\pi}{4}(\gamma(\arcsin(x))))$. After this polynomial is constructed, we can find the corresponding phase factors and implement QSVT, which we refer to [Yin22, DLNW22, DLNW23] for details. Typically, γ is a smooth function of moderate degree, so we may regard m_{γ} and $\deg\gamma$ as O(1) and conclude that the total cost of implementing a $(1,2,\epsilon)$ -block encoding of $\cos(\frac{\pi}{4}\gamma(W))$ is $O(b\log(\frac{1}{\epsilon})^2)$, taking the encoding cost of $\sin(W)$ into account. The $(1,2,\epsilon)$ -block encoding of $\sin(\frac{\pi}{4}\gamma(W))$ follows the same routine, and the only difference is one shall approximate the odd function $\sin(\frac{\pi}{4}(\gamma(\arcsin(x))))$. Using LCU, we can implement a $(\sqrt{2},3,\epsilon)$ -block encoding of $e^{\frac{i}{2}(\pi\beta(D_-)+\pi D_-)}$ within $O(b\log(\frac{1}{\epsilon})^2)$ cost. When measuring the ancilla qubits, we get the desired matrix for probability $\frac{1}{2}$. A naive way to extract the desired unitary matrix is to repeat the whole process until success. However, a better way is to use the "perfect amplitude amplification" [BAG23] to boost the success probability to 1 deterministically with a constant overhead. Therefore, we conclude that we can implement $e^{\frac{i}{2}(\pi\beta(D_-)+\pi D_-)}$ within $O(b\log(\frac{1}{\epsilon})^2) = O(n\log(\frac{1}{\epsilon})^2)$ cost.

2.3. Complexity analysis. The circuit complexity of our Gabor atom implementation is analyzed below, assuming single-qubit and two-qubit gates as elementary building blocks. The circuit of the sharp Gabor atoms, shown in Figure 4, is $O(n^2)$, comprising O(n) operations flanked by two Fourier transform circuits, each with $O(n^2)$ complexity. For blended Gabor atoms, the complexity remains at most O(poly(n)), even if we always use the exact implementations and do not use any ancilla qubit as in Figure 10. For instance, selecting $\beta(x)$ as x or $2x^2$ for $0 \le x \le \frac{1}{2}$ and employing the method in Section 2.2.3 for diagonal matrix implementation still yields $O(n^2)$ complexity, since we can check that each block in Figure 7 costs no more than $O(n^2)$.

If we allow for an ϵ error and use three ancilla qubits, then the overall complexity is only $O(n(\log n + \log(\epsilon^{-1})^2))$. A step-by-step examination of Figure 7 verifies this. The Fourier transform can be performed using an $O(n\log(n\epsilon^{-1}))$ algorithm [NSM20]. $Q_{G(M)}$ has an O(n) complexity since $G_{G(M)}$ is O(n) and L can also be implemented within O(n) complexity using one ancilla qubit [Kla99]. In the implementation of V_G , the multiple qubit controls can be implemented as in Figure 10, and the required diagonal matrices can be implemented within $O(n\log(\epsilon^{-1})^2)$ for general $\beta(x)$ using three ancilla qubits as discussed in Section 2.2.4.

3. Wavelets

This section gives the discretization of the (sharp) Shannon wavelets and (blended) Meyer wavelets and presents the corresponding quantum circuits. The discretization of the Shannon wavelet is straightforward, and its circuit implementation can be viewed as a recursive process. For the Meyer wavelets, a phase adjustment

is necessary to ensure orthogonality when imposing periodic boundary conditions. When implementing its quantum circuit, we first reallocate the Fourier coefficient $\hat{f}(k)$'s into the correct positions and then apply the circuit for the Shannon wavelet, akin to our approach with Gabor atoms. However, the reallocation process involves multiple levels of control, and sometimes the control occurs at $\frac{N}{3\cdot 2^j}$ rather than powers of 2, which makes it more technical.

3.1. Shannon wavelets (sharp). In the continuous setting, the Shannon wavelet basis $\widehat{\psi_{j,p}}$ is given by (1.5) and (1.6). The Fourier transforms of discrete Shannon wavelets are given by

(3.1)
$$\widehat{\psi_{j,p}}(k) = \frac{1}{\sqrt{2^{n-j}}} e^{2\pi i \frac{pk}{2^{n-j}}} \left[\chi_{[-2^{n-j},-2^{n-j-1})}(k) + \chi_{[2^{n-j-1},2^{n-j})}(k) \right],$$

for $j=1,2,\ldots,n$ and $p\in[2^{n-j}]$. In particular, when j=n and p=0, $\widehat{\psi_{j,p}}=\chi_{\{-1\}}$. In addition, the last basis functions are given by the scaling function

$$\widehat{\phi_{n,0}} = \chi_{\{0\}}.$$

We remark that, similar to the sharp Gabor atom case, it holds that $\widehat{\psi_{j,p}}(k) = \sqrt{\frac{2\pi}{N}}\widehat{\psi_{j,p}}(\frac{2\pi}{N}k)$ for $k = -N/2, \dots, N/2 - 1$.

All the $\widehat{\psi_{j,p}}$'s together with $\widehat{\phi_{n,0}}$ form an orthonormal basis of \mathbb{C}^N since the supports of $\widehat{\psi_{j,p}}$ at different level j's are disjoint. Some version of Shannon wavelets may have extra phases multiplied on these $\chi_{[-2^{n-j},-2^{n-j-1})}(k)$ and $\chi_{[2^{n-j-1},2^{n-j})}(k)$ [Mal99, Chapter 7.2], but we do not adopt them here.

By orthogonality, the wavelet coefficients of signal f are

(3.3)
$$a_{j,p} = \langle f, \psi_{j,p} \rangle = \langle \hat{f}, \widehat{\psi_{j,p}} \rangle = \left(\sum_{k=2^{n-j-1}}^{2^{n-j-1}} + \sum_{k=-2^{n-j}}^{-2^{n-j-1}-1} \right) \frac{1}{\sqrt{2^{n-j}}} e^{-2\pi i \frac{pk}{2^{n-j}}} \hat{f}(k).$$

and

(3.4)
$$a_{n+1,0} = \langle f, \phi_{n,0} \rangle = \langle \hat{f}, \widehat{\phi_{n,0}} \rangle = \hat{f}(0).$$

The Shannon wavelet transform is defined as

$$(3.5) \quad U_{\text{WS}}: \mathbb{C}^N \to \mathbb{C}^N: f \mapsto a = (a_{1,0}, \dots, a_{1,N/2-1}, a_{2,0}, \dots, a_{2,N/4-2}, \dots, a_{n-1,0}, a_{n-1,1}, a_{n,0}, a_{n+1,0})^T.$$

Since the calculation (3.3) first involves a Fourier transform of f, we introduce

$$(3.6) S_{W(N)} : \mathbb{C}^N \to \mathbb{C}^N : \hat{f} \mapsto a,$$

which satisfies $U_{WS} = S_{W(N)}U_{FT(N)}$. Notice that when N = 2, $S_{W(2)} = X$ is the Pauli X matrix.

Consider the rearrangement of the index of \hat{f} as follows:

$$G_{W(N)}: (\hat{f}(0), \dots, \hat{f}(N/2-1), \hat{f}(-N/2), \dots, \hat{f}(-1))^{T}$$

$$\mapsto (\hat{f}(-N/2), \dots, \hat{f}(-N/4-1), \hat{f}(N/4), \dots, \hat{f}(N/2-1), \hat{f}(0), \dots, \hat{f}(N/4-1), \hat{f}(-N/4), \dots, \hat{f}(-1))^{T},$$

which is the transposition of the first and the third quarter of the indices. The matrix form of $G_{W(N)}$ can be written explicitly as $G_{W(N)} = P_{1,3} \otimes I_{N/4}$, where

$$P_{1,3} := \begin{bmatrix} 0 & 0 & 1 & 0 \\ 0 & 1 & 0 & 0 \\ 1 & 0 & 0 & 0 \\ 0 & 0 & 0 & 1 \end{bmatrix} = \underbrace{\hspace{1cm}}$$

is just a $|0\rangle$ controlled-NOT gate. After this rearrangement, when j=1, (3.3) becomes

(3.7)
$$a_{1,p} = \sum_{k=0}^{2^{n-1}-1} \frac{1}{\sqrt{2^{n-1}}} e^{-2\pi i \frac{pk}{2^{n-1}}} (G_{W(N)}\hat{f})(k),$$

which is an inverse Fourier transform of size $\frac{N}{2}$ on the first half of $G_{W(N)}\hat{f}$.

Moreover, the latter half of $G_{W(N)}\hat{f}$ is exactly the middle half of \hat{f} , i.e., the second and third quarters of \hat{f} . By definition (3.3), we notice that the second half of the coefficient vector a, denoted as

$$(3.8) a(N/2:N-1) = (a_{2,0}, \dots, a_{2,N/4-2}, \dots, a_{n-1,0}, a_{n-1,1}, a_{n,0}, a_{n,1})^T,$$

only depends on $(G_{W(N)}\hat{f})(N/2:N-1)=\hat{f}(-N/4:N/4-1)$, and this dependence follows the same pattern as (3.3) except for N is replaced by N/2. More specifically,

$$(3.9) S_{W(N/2)}(G_{W(N)}\hat{f})(N/2:N-1) = a(N/2:N-1).$$

Therefore, $S_{\mathrm{W}(N)}$ can be implemented recursively, as shown in Figure 12, and we have

$$(3.10) S_{W(K)} = \left(|0\rangle\langle 0| \otimes U_{FT(K/2)}^{\dagger} + |1\rangle\langle 1| \otimes S_{W(K/2)} \right) G_{W(K)}$$

for $K = N, N/2, N/4, \ldots, 4$, with the base case $S_{W(2)} = X$ being the Pauli X matrix. This can be implemented in the quantum circuit as Figure 13. The fully expanded circuit is shown in Figure 14. This circuit also contains multi-qubit controlled unitary matrices, which can be implemented as in Figure 10.

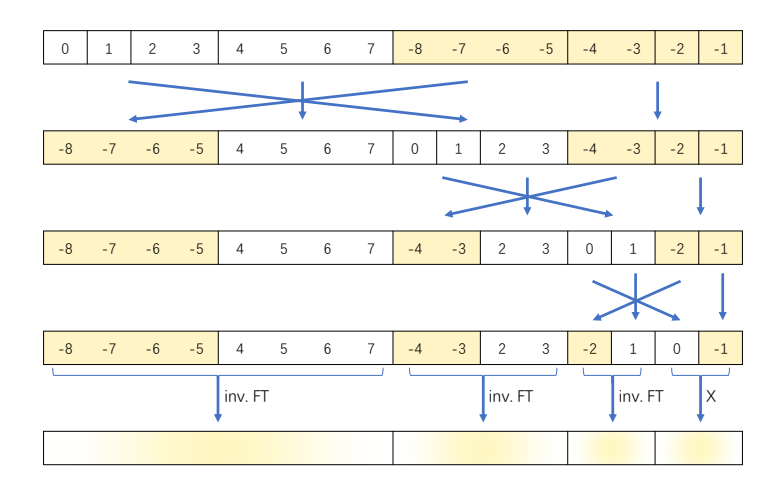


Figure 12. The illustration of $S_{W(K)}$. It contains a reshuffling process, followed by inverse Fourier transforms. The inverse Fourier transforms can also be performed right after the corresponding reshuffling process.

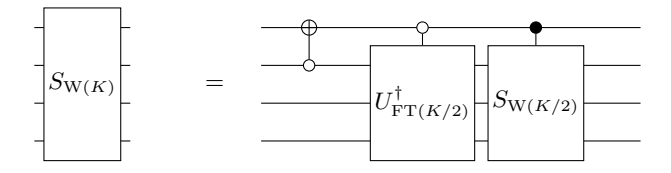


Figure 13. The recursive definition of $S_{W(K)}$. The base case is $S_{W(2)} = X$.

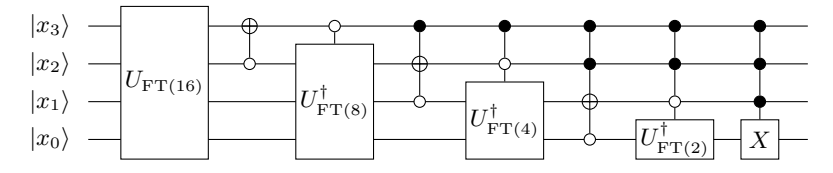


Figure 14. The fully expanded circuit of $U_{\rm WS}$ when N=16. Here, for multiple qubit control gates, the controlling qubits may be located both on the upper wires and lower wires of the controlled qubit.

3.2. Meyer wavelets (blended). In the continuous setting, the Meyer wavelets are given by (1.7). In order to impose a periodic boundary condition here and maintain the orthogonality, we need to introduce a phase shift and define

(3.11)
$$\hat{\psi}_{ms}(\omega) = \begin{cases} e^{i\frac{\pi}{4} - i\frac{\omega}{2}} g\left(\frac{3\omega}{2} - 2\pi\right) & \text{if } \frac{2\pi}{3} \le \omega \le \frac{4\pi}{3}, \\ e^{i\frac{\pi}{4} - i\frac{\omega}{2}} g\left(\frac{3\omega}{4} - \pi\right) & \text{if } \frac{4\pi}{3} \le \omega \le \frac{8\pi}{3}, \\ 0 & \text{if } 0 \le \omega \le \frac{2\pi}{3} \text{ or } \omega \ge \frac{8\pi}{3}, \\ \hat{\psi}_{ms}(-\omega)^* & \text{if } \omega < 0. \end{cases}$$

Now we can define the discrete Meyer wavelet base functions $\psi_{j,p}$ by assigning its Fourier coefficients as

$$\widehat{\psi_{j,p}}(k) = \frac{1}{\sqrt{2^{n-j}}} e^{2\pi i \frac{pk}{2^{n-j}}} \sum_{q \in \mathbb{Z}} \widehat{\psi}_{ms} \left(2^{j+1} \pi \left(\frac{k}{N} + q \right) \right), \quad (k = -\frac{N}{2}, -\frac{N}{2} + 1, \dots, \frac{N}{2} - 1),$$

for j = 1, 2, ..., n and $p \in [2^{n-j}]$. One can check that these N-1 functions, together with the scaling function

$$\widehat{\phi_{n,0}} = \chi_{\{0\}}$$

form an orthonormal basis of \mathbb{C}^N . While the orthogonality can be calculated directly, it can also be seen as a corollary of the following discussions, in which we will illustrate that the expansion under this basis is unitary. When $k=-\frac{N}{2},-\frac{N}{2}+1,\ldots,\frac{N}{2}-1$, (3.12) can also be formulated as

$$\widehat{\psi_{j,p}}(k) = \begin{cases} \frac{1}{\sqrt{2^{n-j}}} e^{2\pi i \frac{pk}{2^{n-j}}} \sum_{q=-1}^{1} \widehat{\psi}_{ms} \left(2^{j+1} \pi \left(\frac{k}{N} + q\right)\right) & \text{if } j = 1, \\ \frac{1}{\sqrt{2^{n-j}}} e^{2\pi i \frac{pk}{2^{n-j}}} \widehat{\psi}_{ms} \left(2^{j+1} \pi \frac{k}{N}\right) & \text{if } j = 2, 3, \dots, n. \end{cases}$$

We also point out that if we ignore the range of k in (3.12), it still holds $\widehat{\psi_{j,p}}(k) = \widehat{\psi_{j,p}}(k+N)$, which is compatible with our convention. Our objective is to calculate the wavelet coefficients

$$(3.15) a_{i,p} = \langle f, \psi_{i,p} \rangle = \langle \hat{f}, \widehat{\psi_{i,p}} \rangle$$

and

(3.16)
$$a_{n+1,0} := \langle f, \phi_{n,0} \rangle = \langle \hat{f}, \widehat{\phi_{n,0}} \rangle = \hat{f}(0).$$

Then the wavelet transform in a matrix form is

$$(3.17) \quad U_{\text{WB}}: \mathbb{C}^N \to \mathbb{C}^N: f \mapsto a = (a_{1,0}, \dots, a_{1,N/2-1}, a_{2,0}, \dots, a_{2,N/4-2}, \dots, a_{n-1,0}, a_{n-1,1}, a_{n,0}, a_{n+1,0})^T.$$

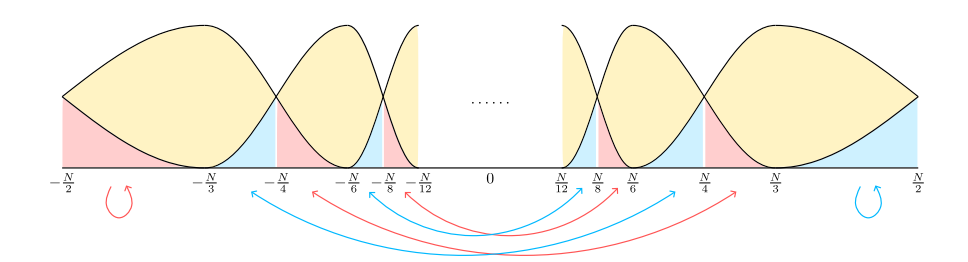


Figure 15. This figure demonstrates the reallocations of $\hat{f}(k)$ in the first few levels. $\widehat{\psi_{j,p}}$ is shown as two bumps supported at $\left[-\frac{2^{n-j+2}}{3}, -\frac{2^{n-j}}{3}\right)$ and $\left[\frac{2^{n-j}}{3}, \frac{2^{n-j+2}}{3}\right)$. After the transpositions, the relevant $\hat{f}(k)$'s would be placed at $\left[-2^{n-j}, -2^{n-j-1}\right] \cup \left[2^{n-j-1}, 2^{n-j}\right]$ with correct proportions.

Similar to the blended Gabor atom case, the support of basis functions at adjacent levels are overlapping. Therefore, we reallocate a portion of each $\hat{f}(k)$, which is illustrated in Figure 15. To write down this reallocation process precisely, we introduce an intermediate variable $h \in \mathbb{C}^N$, which is given by

$$(3.18) \qquad h(\frac{N}{2^{j}}-q) = -e^{-i\frac{\pi}{4}-i\frac{\pi q2^{j}}{N}}g(\frac{\pi}{2}-\frac{3\pi q2^{j-1}}{N})\hat{f}(\frac{N}{2^{j}}-q) - e^{i\frac{\pi}{4}-i\frac{\pi q2^{j}}{N}}g(-\frac{\pi}{2}-\frac{3\pi q2^{j-1}}{N})\hat{f}(-\frac{N}{2^{j}}-q),$$

$$(3.19) \quad h(-\frac{N}{2^{j}}-q) = e^{i\frac{\pi}{4}-i\frac{\pi q 2^{j-1}}{N}}g(-\frac{\pi}{2}-\frac{3\pi q 2^{j-1}}{N})\hat{f}(\frac{N}{2^{j}}-q) + e^{-i\frac{\pi}{4}-i\frac{\pi q 2^{j-1}}{N}}g(\frac{\pi}{2}-\frac{3\pi q 2^{j-1}}{N})\hat{f}(-\frac{N}{2^{j}}-q),$$

for $j=2,3,\cdots,n$ and $1\leq q<\frac{N}{3\cdot 2^j}$. Similarly, we define

$$(3.20) \quad h(\frac{N}{2^{j}}+q) = e^{i\frac{\pi}{4} + i\frac{\pi q2^{j-1}}{N}}g(-\frac{\pi}{2} + \frac{3\pi q2^{j-1}}{N})\hat{f}(\frac{N}{2^{j}}+q) + e^{-i\frac{\pi}{4} + i\frac{\pi q2^{j-1}}{N}}g(\frac{\pi}{2} + \frac{3\pi q2^{j-1}}{N})\hat{f}(-\frac{N}{2^{j}}+q),$$

$$(3.21) \quad h(-\frac{N}{2^{j}}+q) = -e^{-i\frac{\pi}{4} + i\frac{\pi q2^{j}}{N}}g(\frac{\pi}{2} + \frac{3\pi q2^{j-1}}{N})\hat{f}(\frac{N}{2^{j}}+q) - e^{i\frac{\pi}{4} + i\frac{\pi q2^{j}}{N}}g(-\frac{\pi}{2} + \frac{3\pi q2^{j-1}}{N})\hat{f}(-\frac{N}{2^{j}}+q),$$

for
$$j = 2, 3, \dots, n$$
 and $0 \le q < \frac{N}{3 \cdot 2^{j}}$.

For the first level j=1, there is a little bit of difference since there is no higher level and the indices $-\frac{N}{2}+q$ and $\frac{N}{2}+q$ are the same. Therefore, we only adopt (3.18) and (3.21) for j=1 and $0 \le q < \frac{N}{3 \cdot 2^j}$. Finally, let $h(0) = \hat{f}(0)$ for the scaling function component. We denote this transformation from \hat{f} to h as $T_{\rm W}$, which is $h = T_{\rm W} \hat{f}$.

We may calculate that

(3.22)
$$\left(\sum_{k=2^{n-j-1}}^{2^{n-j}-1} + \sum_{k=-2^{n-j}}^{-2^{n-j-1}-1}\right) \frac{1}{\sqrt{2^{n-j}}} e^{-2\pi i \frac{pk}{2^{n-j}}} h(k) = \langle \hat{f}, \widehat{\psi_{j,p}} \rangle = a_{j,p}.$$

The proof is in Section 4.2. Noticing that the left-hand side of (3.22) is exactly the same as applying $S_{W(N)}$ on h, we conclude

$$(3.23) U_{WB} = S_{W(N)} T_W U_{FT(N)}.$$

Therefore, the only remaining problem is to implement the matrix T_{W} .

3.3. The implementation of T_W . The idea of implementing T_W is similar to T_G in the Gabor atom implementation, exploiting the block diagonal structure and using the technique of encoding the exponential of pure imaginary polynomials. However, the main challenge here is the ranges of indices are not power of 2. A plausible choice to get around this difficulty is to further restrict the support of g(x) to $\left[-\frac{7\pi}{8}, \frac{7\pi}{8}\right]$, and also adjust the phase rotation factors $e^{-i\frac{\omega}{2}}$ in (1.7) in order to restrict the non-trivial part of the operations in blocks of size of power of 2. However, because this choice makes the wavelet different from what is commonly used, we choose to present a method that can implement T_W without any restrictions.

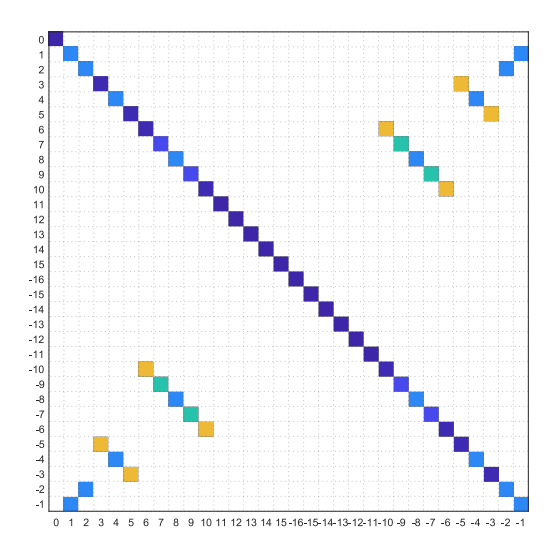


Figure 16. Magnitude of elements in $T_{\rm W}$ with N=32.

From the formulas (3.18) - (3.21), we see that $T_{\rm W}$ has a block-diagonal structure. This can also be seen from Figure 16. Let us write the unitary block explicitly as

(3.24)
$$T_{W} = \prod_{j=1}^{n} R_{j} \prod_{j=1}^{n} L_{j}$$

where R_j is the unitary corresponding to (3.20) and (3.21) for level j, and L_j is the unitary corresponding to (3.18) and (3.19) for level j. Notice that R_1 and L_1 are only defined by (3.21) and (3.18), respectively. Since the support of all R_j 's and L_j 's are disjoint, they are all commutative, and thus the order of product does not matter.

By definition, R_j is acting non-trivially on the indices $\pm \frac{N}{2^j} + q$ for $0 \le q < \frac{N}{3 \cdot 2^j}$. However, this range is not convenient for quantum implementation since it is not a power of 2. Therefore, we may first enlarge the range of q to $0 \le q < \frac{N}{2^j}$ and pad the extra slots by identity. In the binary representation, this range contains the binary strings beginning with $\underbrace{0 \cdots 01}_{(j-1) \text{ of 0's}}$ and $\underbrace{1 \cdots 11}_{(j-1) \text{ of 1's}}$. When $j \ge 2$, we shall first group these two ranges

together and then perform the desired unitary transformation. To be specific, we need a permutation matrix $Q_{W(2^j)}$ such that

$$(3.25) Q_{W(2^j)} \mid \underbrace{0 \cdots 0}_{(j-1) \text{ of 0's}} 1 \rangle = \mid \underbrace{1 \cdots 1}_{(j-1) \text{ of 1's}} 0 \rangle \quad \text{and} \quad Q_{W(2^j)} \mid \underbrace{1 \cdots 1}_{(j-1) \text{ of 1's}} 1 \rangle = \mid \underbrace{1 \cdots 1}_{(j-1) \text{ of 1's}} 1 \rangle.$$

There are different choices of $Q_{W(2^j)}$, and we adopt the following

$$|x_{n-1}x_{n-2}\cdots x_{n-j+1}x_{n-j}\rangle$$

$$(3.26) \qquad \mapsto |x_{n-1}(x_{n-2}\oplus x_{n-1}\oplus 1)\cdots (x_{n-j+1}\oplus x_{n-1}\oplus 1)(x_{n-j}\oplus x_{n-1}\oplus 1)\rangle$$

$$\mapsto |(x_{n-j}\oplus x_{n-1}\oplus 1)(x_{n-2}\oplus x_{n-1}\oplus 1)\cdots (x_{n-j+1}\oplus x_{n-1}\oplus 1)x_{n-1}\rangle$$

which is illustrated in Figure 17.

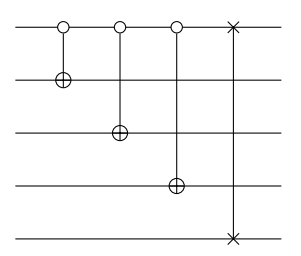


Figure 17. The circuit for $Q_{W(32)}$.

After applying $Q_{W(2^j)}$, the relevant indices begin with $\underbrace{1\cdots 1}_{(j-1) \text{ of 1's}} 0$ and $\underbrace{1\cdots 1}_{(j-1) \text{ of 1's}} 1$. Therefore, when $j\geq 2$, the

matrix R_i can be written as

$$(3.27) R_j = (Q_{W(2^j)}^{\dagger} \otimes I_{2^{n-j}})(I_{N-2^{n-j+1}} \oplus K_{2^{n-j+1}})(Q_{W(2^j)} \otimes I_{2^{n-j}})$$

where $K_{2^{n-j+1}}$ is a 2^{n-j+1} dimensional matrix that can be determine according to (3.20) and (3.21). Let D be a $\lceil \frac{N}{3 \cdot 2^j} \rceil$ dimensional diagonal matrix $D = \text{diag}\{-\frac{1}{2} + \frac{3q2^{j-1}}{N} : 0 \le q < \frac{N}{3 \cdot 2^j}\}$, then

(3.28)
$$K_{2^{n-j+1}} = \begin{bmatrix} e^{i\pi(\frac{1}{3}D + \frac{5}{12})}\cos(\frac{\pi}{2}\beta(D)) & 0 & -e^{i\pi(\frac{1}{3}D - \frac{1}{12})}\sin(\frac{\pi}{2}\beta(D)) & 0\\ 0 & I & 0 & 0\\ e^{i\pi(\frac{2}{3}D + \frac{1}{12})}\sin(\frac{\pi}{2}\beta(D)) & 0 & -e^{i\pi(\frac{2}{3}D + \frac{7}{12})}\cos(\frac{\pi}{2}\beta(D)) & 0\\ 0 & 0 & 0 & I \end{bmatrix},$$

where I stands for the $\frac{N}{2^j} - \lceil \frac{N}{3 \cdot 2^j} \rceil$ dimensional identity matrix. Note that as this matrix only depends on the value of n - j, it makes sense to write $K_{2^{m+1}}$ without specifying n and j.

When j = 1, the matrix R_1 is different from the (3.27). According to (3.21), we have

$$(3.29) R_1 = I_{N/2} \oplus \widetilde{K_{N/2}}$$

with

(3.30)
$$\widetilde{K_{N/2}} = \begin{bmatrix} e^{i\pi(-\frac{5}{12} + \frac{2}{3}D + \frac{1}{2}\beta(D))} & 0\\ 0 & I \end{bmatrix},$$

where $D = \text{diag}\{-\frac{1}{2} + \frac{3q}{N} : 0 \le q < \frac{N}{6}\}$, and I stands for the $\frac{N}{2} - \lceil \frac{N}{6} \rceil$ dimensional identity matrix.

Next, we focus on implementing (3.27) and (3.30). We first discuss the latter one since it has a more simple form. The idea is to use an ancilla qubit to filter the binary representations of numbers smaller than $\frac{N}{6}$. Recall that $\widetilde{K_{N/2}}$ is of dimension $\frac{N}{2}$ and the largest number less than $\frac{N}{6}$ is given by the binary representation $\underbrace{0101\cdots}_{(n-1) \text{ bits}}$. Therefore, all numbers less than $\frac{N}{6}$ have the binary representation begin with 00, or 0100, or

010100, or so on. Once we use control gates to encode these conditional statements into the ancilla qubit, we can perform a controlled version of $e^{i\pi(-\frac{5}{12}+\frac{2}{3}D_p+\frac{1}{2}\beta(D_p))}$, where D_p is the padded version of D_p , namely $D_p = \text{diag}\{-\frac{1}{2}+\frac{3q}{N}: 0 \leq q < \frac{N}{2}\}$. This D_p can be implemented using the method discussed in Section 2.2.3. Finally, one should go through the uncompute process to restore the ancilla to $|0\rangle$ and discard it. The complete circuit is shown in Figure 18.

Next, let us construct the circuit of matrix $K_{2^{n-j+1}}$. We similarly introduce the padded diagonal matrix $D_p = \text{diag}\{-\frac{1}{2} + \frac{3q2^{j-1}}{N} : 0 \le q < \frac{N}{2^j}\}$. One may also introduce an ancilla qubit to record whether the binary number given by the last n-j qubits is less than $\frac{N}{3\cdot 2^j}$. Therefore, under the control of the ancilla qubit, the matrix to be implemented is

$$\begin{bmatrix}
e^{i\pi(\frac{1}{3}D_p + \frac{5}{12})}\cos(\frac{\pi}{2}\beta(D_p)) & -e^{i\pi(\frac{1}{3}D_p - \frac{1}{12})}\sin(\frac{\pi}{2}\beta(D_p)) \\
e^{i\pi(\frac{2}{3}D_p + \frac{1}{12})}\sin(\frac{\pi}{2}\beta(D_p)) & -e^{i\pi(\frac{2}{3}D_p + \frac{7}{12})}\cos(\frac{\pi}{2}\beta(D_p))
\end{bmatrix}$$

which can be further decomposed as

$$\left[e^{i\pi(\frac{1}{3}D_p + \frac{5}{12})} \quad 0 \atop 0 \quad e^{i\pi(\frac{2}{3}D_p - \frac{5}{12})} \right] \left[\frac{I}{\sqrt{2}} \quad \frac{I}{\sqrt{2}} \right] \left[e^{\frac{i\pi}{2}\beta(D_p)} \quad 0 \atop 0 \quad e^{-\frac{i\pi}{2}\beta(D_p)} \right] \left[\frac{I}{\sqrt{2}} \quad \frac{I}{\sqrt{2}} \right].$$

These four unitary matrices are either Hadamard gates or the exponentials of pure imaginary polynomials, which are constructed in Section 2.2.3. Therefore, we only need to perform the controlled version of them and finally do the uncomputation. The complete circuit is shown in Figure 19.

Having described the implementation of all the building blocks, we conclude by drawing the circuit of $\prod_{j=1}^{n} R_j = R_n R_{n-1} \cdots R_1$ in Figure 20. Note that there would be cancellations at the consecutive $(Q_{W(2^{j+1})}^{\dagger} \otimes I_{2^{n-j-1}})(Q_{W(2^j)} \otimes I_{2^{n-j}})$, which saves some gates.

For the implementation of $\prod_{j=1}^{n} L_j$, the method of implementation is very similar to $\prod_{j=1}^{n} R_j$. Therefore, we omit the details.

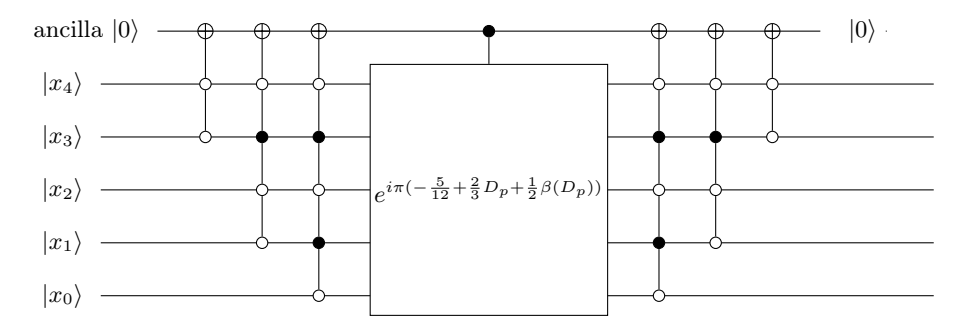


Figure 18. The circuit for K_{32} .

3.4. Complexity analysis. Here, we briefly discuss the complexity of the quantum wavelet transform circuits. For the exact implementation, the complexity is of O(poly(n)), and the degree may depend on the degree of β , which is similar to the Gabor atom case.

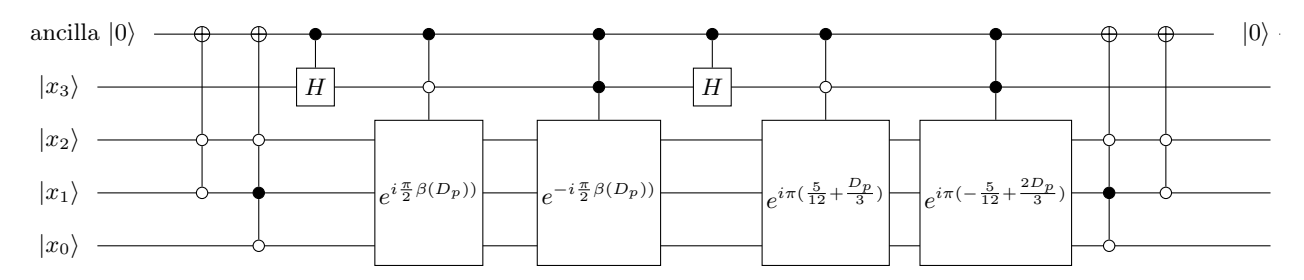


Figure 19. The circuit for K_{16} .

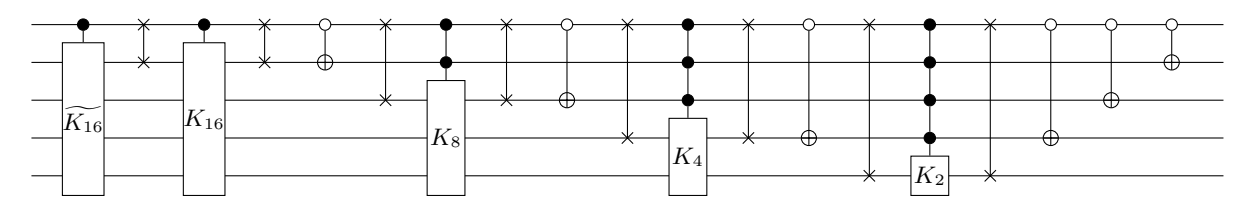


Figure 20. The circuit of $\prod_{j=1}^{n} R_j$ when N=32.

If we allow for an ϵ error, it is possible to reduce the complexity as in the Gabor atom case. In particular, we may use the inexact Fourier transform [NSM20], implement the multi-qubit control by Figure 10, and implement the required diagonal matrices using the method in Section 2.2.4. For the Shannon wavelet, the corresponding complexity is $O(n^2 \log(n\epsilon^{-1}))$ since we need to perform n (inverse) Fourier transforms. For the Meyer wavelet, we claim that the complexity is $O(n^2(\log n + \log(\epsilon^{-1})^2))$ by examining each term in (3.23) as follows. The $S_{W(N)}$ is of complexity $O(n^2 \log(n\epsilon^{-1}))$ as discussed in the Shannon wavelet. The T_W part is mainly composed of implementing O(n) diagonal matrices, and each of them costs $O(n \log(\epsilon^{-1})^2)$ as discussed in Section 2.2.4.

Notice that for the implementation of a required diagonal matrix, one needs an ancilla qubit, as shown in Figure 18 and Figure 19. At the same time, one extra ancilla qubit is needed for unwrapping the multi-qubit control on the diagonal matrices. Therefore, in total two extra ancilla qubits are required.

4. Proofs

4.1. **Proof of Equation (2.17).** We may further split the sum of the left-hand side into four terms

$$(4.1) \qquad \left(\sum_{k \in [jB,(j+\frac{1}{2})B)} + \sum_{k \in [(j+\frac{1}{2})B,(j+1)B)} + \sum_{k \in [-(j+1)B,-(j+\frac{1}{2})B)} + \sum_{k \in [-(j+\frac{1}{2})B,-jB)} \right) \frac{1}{\sqrt{2B}} e^{-2\pi i \frac{pk}{2B}} h(k).$$

The right-hand side is the sum on the support of $\widehat{\psi_{2Bj+p}}$

$$\langle \hat{f}, \widehat{\psi_{2Bj+p}} \rangle = \left(\sum_{k \in [(j-\frac{1}{2})B, (j+\frac{3}{2})B)} + \sum_{k \in [-(j+\frac{3}{2})B, -(j+\frac{1}{2})B)} \widehat{f}(k) \widehat{\psi_{2Bj+p}}(k)^* \right)$$

$$= \left(\sum_{\substack{k \in [jB, (j+\frac{1}{2})B) \\ \cup [-jB, (-j+\frac{1}{2})B)}} + \sum_{\substack{k \in [(j+\frac{1}{2})B, (j+1)B) \\ \cup [-(j+\frac{3}{2})B, -(j+1)B)}} + \sum_{\substack{k \in [-(j+1)B, -(j+\frac{1}{2})B) \\ \cup [(j+1)B, (j+\frac{3}{2})B)}} + \sum_{\substack{k \in [-(j+\frac{1}{2})B, -jB) \\ \cup [(j-\frac{1}{2})B, jB)}} \widehat{f}(k) \widehat{\psi_{2Bj+p}}(k)^*.$$

Using the definition of h, we can check that the four summations in (4.1) and (4.2) are equal, respectively. For instance, the first summation

$$\sum_{\substack{k \in [jB,(j+\frac{1}{2})B) \\ \cup [-jB,(-j+\frac{1}{2})B)}} \hat{f}(k)\widehat{\psi_{2Bj+p}}(k)^*$$

$$= \sum_{\substack{q \in [0,\frac{B}{2})}} \hat{f}(jB+q)\widehat{\psi_{2Bj+p}}(jB+q)^* + \sum_{\substack{q \in [0,\frac{B}{2})}} \hat{f}(-jB+q)\widehat{\psi_{2Bj+p}}(-jB+q)^*$$

$$= \sum_{\substack{q \in [0,\frac{B}{2})}} \hat{f}(jB+q)\frac{1}{\sqrt{2B}}e^{-2\pi i\frac{p(jB+q)}{2B}}e^{\frac{i}{2}(-\frac{\pi}{2}+q\frac{\pi}{B})}g\left(-\frac{\pi}{2}+q\frac{\pi}{B}\right)$$

$$+ \sum_{\substack{q \in [0,\frac{B}{2})}} \hat{f}(-jB+q)\frac{1}{\sqrt{2B}}e^{-2\pi i\frac{p(-jB+q)}{2B}}e^{\frac{i}{2}(\frac{\pi}{2}+q\frac{\pi}{B})}g\left(\frac{\pi}{2}+q\frac{\pi}{B}\right)$$

$$= \sum_{\substack{q \in [0,\frac{B}{2})}} \frac{1}{\sqrt{2B}}e^{-2\pi i\frac{p(jB+q)}{2B}}h(jB+q) \quad \text{(used (2.15))}$$

$$= \sum_{\substack{k \in [jB,(j+\frac{1}{2})B)}} \frac{1}{\sqrt{2B}}e^{-2\pi i\frac{pk}{2B}}h(k).$$

The other three summations can be checked similarly. Therefore, we have proved Equation (2.17).

4.2. **Proof of Equation (3.22).** To verify this, we may further split the sum of the left-hand side into (4.4)

$$\left(\sum_{k\in\left[-\frac{4}{3}2^{n-j-1},-2^{n-j-1}\right)} + \sum_{k\in\left[-2^{n-j},-\frac{2}{3}2^{n-j}\right)} + \sum_{k\in\left[\frac{2}{3}2^{n-j},2^{n-j}\right)} + \sum_{k\in\left[2^{n-j-1},\frac{4}{3}2^{n-j-1}\right)} \frac{1}{\sqrt{2^{n-j}}} e^{-2\pi i \frac{pk}{2^{n-j}}} h(k).$$

The right-hand side is the sum on the support of $\widehat{\psi_{j,p}}$

$$\langle \widehat{f}, \widehat{\psi_{j,p}} \rangle = \left(\sum_{k \in [\frac{2}{3}2^{n-j-1}, \frac{4}{3}2^{n-j})} + \sum_{k \in [-\frac{4}{3}2^{n-j}, -\frac{2}{3}2^{n-j-1})} \right) \widehat{f}(k) \widehat{\psi_{j,p}}(k)^*$$

$$= \left(\sum_{k \in [-\frac{4}{3}2^{n-j-1}, -2^{n-j-1})} + \sum_{k \in [-2^{n-j}, -\frac{2}{3}2^{n-j})} + \sum_{k \in [\frac{2}{3}2^{n-j}, 2^{n-j})} + \sum_{k \in [2^{n-j-1}, \frac{4}{3}2^{n-j-1})} \right) \widehat{f}(k) \widehat{\psi_{j,p}}(k)^*.$$

$$(4.5)$$

$$= \left(\sum_{k \in [-\frac{4}{3}2^{n-j-1}, -2^{n-j-1})} + \sum_{k \in [-2^{n-j}, -\frac{2}{3}2^{n-j})} + \sum_{k \in [\frac{2}{3}2^{n-j}, 2^{n-j})} + \sum_{k \in [2^{n-j-1}, \frac{4}{3}2^{n-j-1})} \widehat{f}(k) \widehat{\psi_{j,p}}(k)^*.$$

We shall show the four summations in (4.4) and (4.5) are equal, respectively. For the first summation, we have

$$\begin{aligned} &\sum_{k \in \left[-\frac{4}{3}2^{n-j-1}, -2^{n-j-1}\right)} \hat{f}(k) \widehat{\psi_{j,p}}(k)^* \\ &= \sum_{q \in \left(0, \frac{1}{3}2^{n-j-1}, 2^{n-j-1}\right)} \hat{f}(-2^{n-j-1} - q) \widehat{\psi_{j,p}}(-2^{n-j-1} - q)^* + \sum_{q \in \left(0, \frac{1}{3}2^{n-j-1}\right]} \hat{f}(2^{n-j-1} - q) \widehat{\psi_{j,p}}(2^{n-j-1} - q)^* \\ &= \sum_{q \in \left(0, \frac{1}{3}2^{n-j-1}\right]} \frac{1}{\sqrt{2^{n-j}}} \hat{f}(-2^{n-j-1} - q) e^{2\pi i p(-2^{n-j-1} - q)/2^{n-j}} \hat{\psi}_{ms}(2^{j+1-n} \pi(-2^{n-j-1} - q))^* \\ &+ \sum_{q \in \left(0, \frac{1}{3}2^{n-j-1}\right]} \frac{1}{\sqrt{2^{n-j}}} \hat{f}(2^{n-j-1} - q) e^{2\pi i p(2^{n-j-1} - q)/2^{n-j}} \hat{\psi}_{ms}(2^{j+1-n} \pi(2^{n-j-1} - q))^* \\ &= \sum_{q \in \left(0, \frac{1}{3}2^{n-j-1}\right]} \frac{1}{\sqrt{2^{n-j}}} \hat{f}(-2^{n-j-1} - q) e^{2\pi i p(-2^{n-j-1} - q)/2^{n-j}} e^{-i\frac{\pi}{4} - i\frac{\pi q2^j}{N}} g(\frac{\pi}{2} - \frac{3\pi q2^j}{N}) \\ &+ \sum_{q \in \left(0, \frac{1}{3}2^{n-j-1}\right]} \frac{1}{\sqrt{2^{n-j}}} \hat{f}(2^{n-j-1} - q) e^{2\pi i p(2^{n-j-1} - q)/2^{n-j}} e^{i\frac{\pi}{4} - i\frac{\pi q2^j}{N}} g(-\frac{\pi}{2} - \frac{3\pi q2^j}{N}) \\ &= \sum_{q \in \left(0, \frac{1}{3}2^{n-j-1}\right]} \frac{1}{\sqrt{2^{n-j}}} e^{2\pi i p(-2^{n-j-1} - q)/2^{n-j}} h(-2^{n-j-1} - q) \\ &= \sum_{k \in \left[-\frac{4}{3}2^{n-j-1}, -2^{n-j-1}\right]} \frac{1}{\sqrt{2^{n-j}}} e^{-2\pi i \frac{pk}{2^{n-j}}} h(k). \end{aligned}$$

Therefore, the first summation in (4.4) and (4.5) are equal. The remaining three summations are also equal, respectively, by a similar argument. Thus, we have proved (3.22).

5. Conclusion and Discussions

This paper presents the quantum circuit implementation of wave packets, such as Gabor atoms and wavelets, with compact frequency support. The implementations for those with sharp frequency windows are rather straightforward, with the help of quantum Fourier transform. For those with blended frequency windows, our method first reallocates the Fourier coefficients to the correct location in the frequency domain, followed by applying the transformation for the sharp-windowed versions.

There are many other kinds of wave packets, such as wave atoms [DY07] and curvelets [CD05], which give tiling in space-frequency diagram different from Figure 1. Our method can be extended to accommodate these wave packets as well. Another possible future direction is about higher-dimensional wave packet transforms, which could find applications in solving wave equations or the Schrödinger equation. While 2D or 3D versions of compactly supported wavelets have been discussed [LFP+22, LLX23], little has been explored regarding Meyer-type wavelets or wave packets in higher dimensions.

Another more detailed possible improvement is in the implementation of the unitary diagonal matrices discussed in Section 2.2.4. We anticipate the complexity can be reduced to $O(n\log(\epsilon^{-1}))$. Additionally, considering that QSVT can potentially handle complex polynomials directly rather than splitting them into real and imaginary parts and using LCU to combine them [GSLW18], it may be feasible to find a polynomial that can approximate the even function $e^{-\frac{i\pi}{4}\gamma(\arcsin(x))}$ directly while satisfying the conditions in [GSLW18, Theorem 4]. The QET-U technique [DLT22] may also help since we start from a unitary matrix e^{iD_-} .

References

[BAG23] Mohsen Bagherimehrab and Alan Aspuru-Guzik, Efficient quantum algorithm for all quantum wavelet transforms, arXiv preprint arXiv:2309.09350 (2023).

- [BBC⁺95] Adriano Barenco, Charles H Bennett, Richard Cleve, David P DiVincenzo, Norman Margolus, Peter Shor, Tycho Sleator, John A Smolin, and Harald Weinfurter, *Elementary gates for quantum computation*, Phys. Rev. A **52** (1995), no. 5, 3457.
- [BNWAG23] Mohsen Bagherimehrab, Kouhei Nakaji, Nathan Wiebe, and Alán Aspuru-Guzik, Fast quantum algorithm for differential equations, arXiv preprint arXiv:2306.11802 (2023).
 - [CD03] Emmanuel Candes and Laurent Demanet, Curvelets and fourier integral operators, Comptes rendus. Mathématique **336** (2003), no. 5, 395–398.
 - [CD05] Emmanuel J Candes and Laurent Demanet, The curvelet representation of wave propagators is optimally sparse, Communications on Pure and Applied Mathematics 58 (2005), no. 11, 1472–1528.
- [CGFUPSRG23] F. A. Chaurra-Gutierrez, C. Feregrino-Uribe, J. C. Perez-Sansalvador, and G. Rodriguez-Gomez, Qist: One-dimensional quantum integer wavelet s-transform, Information Sciences 622 (2023), 999–1013.
 - [CLVBY22] Daan Camps, Lin Lin, Roel Van Beeumen, and Chao Yang, Explicit quantum circuits for block encodings of certain sparse matrices, arXiv preprint arXiv:2203.10236 (2022).
 - [CSCG20] S. Chakraborty, S. H. Shaikh, A. Chakrabarti, and R. Ghosh, An image denoising technique using quantum wavelet transform, International Journal of Theoretical Physics 59 (2020), no. 11, 3348–3371.
 - [DLNW22] Yulong Dong, Lin Lin, Hongkang Ni, and Jiasu Wang, Infinite quantum signal processing, arXiv preprint arXiv:2209.10162 (2022).
 - [DLNW23] ______, Robust iterative method for symmetric quantum signal processing in all parameter regimes, arXiv preprint arXiv:2307.12468 (2023).
 - [DLT22] Yulong Dong, Lin Lin, and Yu Tong, Ground-state preparation and energy estimation on early fault-tolerant quantum computers via quantum eigenvalue transformation of unitary matrices, PRX Quantum 3 (2022), no. 4, 040305.
 - [DY07] Laurent Demanet and Lexing Ying, Wave atoms and sparsity of oscillatory patterns, Applied and Computational Harmonic Analysis 23 (2007), no. 3, 368–387.
 - [DY09] _____, Wave atoms and time upscaling of wave equations, Numerische Mathematik 113 (2009), 1–71.
 - [FW99] Amir Fijany and Colin P Williams, Quantum wavelet transforms: Fast algorithms and complete circuits, Quantum Computing and Quantum Communications: First NASA International Conference, QCQC'98 Palm Springs, California, USA February 17–20, 1998 Selected Papers, Springer, 1999, pp. 10–33.
 - [GSLW18] András Gilyén, Yuan Su, Guang Hao Low, and Nathan Wiebe, Quantum singular value transformation and beyond: exponential improvements for quantum matrix arithmetics, arXiv:1806.01838 (2018).
 - [GZL22] C. Gao, R. G. Zhou, and X. Li, A quantum steganography scheme using quantum wavelet transforms, Modern Physics Letters B **36** (2022), no. 19, 18.
 - [HNG⁺17] S. Heidari, M. Naseri, R. Gheibi, M. Baghfalaki, M. R. Pourarian, and A. Farouk, *A new quantum watermarking based on quantum wavelet transforms*, Communications in Theoretical Physics **67** (2017), no. 6, 732–742.
 - [JUIL⁺23] M. Jeng, S. I. Ul Islam, D. Levy, A. Riachi, M. Chaudhary, M. A. I. Nobel, D. Kneidel, V. Jha, J. Bauer, A. Maurya, N. Mahmud, and E. El-Araby, *Improving quantum-to-classical data decoding using optimized quantum wavelet transform*, Journal of Supercomputing 79 (2023), no. 18, 20532–20561.
 - [KDPE+22] B. T. Kiani, G. De Palma, D. Englund, W. Kaminsky, M. Marvian, and S. Lloyd, *Quantum advantage for differential equation analysis*, Physical Review A **105** (2022), no. 2, 15.
 - [Kla99] Andreas Klappenecker, Wavelets and wavelet packets on quantum computers, Wavelet Applications in Signal and Image Processing VII, vol. 3813, SPIE, 1999, pp. 703–713.
 - [LFP+22] H. S. Li, P. Fan, H. L. Peng, S. X. Song, and G. L. Long, Multilevel 2-d quantum wavelet transforms, Ieee Transactions on Cybernetics 52 (2022), no. 8, 8467–8480.
 - [LFX⁺18] H. S. Li, P. Fan, H. Y. Xia, S. X. Song, and X. J. He, *The multi-level and multi-dimensional quantum wavelet packet transforms*, Scientific Reports 8 (2018), 23.

- [LFXS19] H. S. Li, P. Fan, H. Y. Xia, and S. X. Song, Quantum multi-level wavelet transforms, Information Sciences **504** (2019), 113–135.
 - [Lin22a] Lin Lin, Lecture notes on quantum algorithms for scientific computation, arXiv preprint arXiv:2201.08309 (2022).
 - [Lin22b] _____, Lecture notes on quantum algorithms for scientific computation, arXiv:2201.08309 (2022).
 - [Liu09] Yi-Kai Liu, Quantum algorithms using the curvelet transform, Proceedings of the forty-first annual ACM symposium on Theory of computing, 2009, pp. 391–400.
 - [LLX23] H. S. Li, G. Q. Li, and H. Y. Xia, *Three-dimensional quantum wavelet transforms*, Frontiers of Computer Science 17 (2023), no. 5, 14.
 - [LM04] Stéphane Lintner and François Malgouyres, Solving a variational image restoration model which involves l^{∞} constraints, Inverse Problems **20** (2004), no. 3, 815.
- [LNY23] Haoya Li, Hongkang Ni, and Lexing Ying, On efficient quantum block encoding of pseudo-differential operators, Quantum 7 (2023), 1031.
- [Mal99] Stéphane Mallat, A wavelet tour of signal processing, Elsevier, 1999.
- [MBDJ20] A. Moshtaghpour, J. M. Bioucas-Dias, and L. Jacques, Close encounters of the binary kind: Signal reconstruction guarantees for compressive hadamard sampling with haar wavelet basis, Ieee Transactions on Information Theory 66 (2020), no. 11, 7253–7273.
- [MWB⁺23] X. Y. Mu, H. W. Wang, R. Y. Bao, S. M. Wang, and H. Y. Ma, An improved quantum watermarking using quantum haar wavelet transform and qsobel edge detection, Quantum Information Processing 22 (2023), no. 5, 22.
 - [NC00] Michael A Nielsen and Isaac Chuang, Quantum computation and quantum information, 2000.
 - [NSM20] Yunseong Nam, Yuan Su, and Dmitri Maslov, Approximate quantum fourier transform with o (n log (n)) t gates, NPJ Quantum Information 6 (2020), no. 1, 26.
- [SWL⁺13] X. H. Song, S. Wang, S. Liu, A. Abd El-Latif, and X. M. Niu, A dynamic watermarking scheme for quantum images using quantum wavelet transform, Quantum Information Processing 12 (2013), no. 12, 3689–3706.
- [YGMW23] Y. M. Yu, J. Gao, X. Y. Mu, and S. M. Wang, Adaptive lsb quantum image watermarking algorithm based on haar wavelet transforms, Quantum Information Processing 22 (2023), no. 5, 21.
 - [Yin22] Lexing Ying, Stable factorization for phase factors of quantum signal processing, Quantum 6 (2022), 842.
 - [YIVA16] F. Yan, A. M. Iliyasu, and S. E. Venegas-Andraca, A survey of quantum image representations, Quantum Information Processing 15 (2016), no. 1, 1–35.
 - [ZHGZ20] N. R. Zhou, L. X. Huang, L. H. Gong, and Q. W. Zeng, Novel quantum image compression and encryption algorithm based on dqwt and 3d hyper-chaotic henon map, Quantum Information Processing 19 (2020), no. 9, 21.
 - [ZK22] Z. G. Zhang and M. A. Kon, Wavelet matrix operations and quantum transforms, Applied Mathematics and Computation 428 (2022), 26.
 - [ZYI+22] S. Zhao, F. Yan, A. M. Iliyasu, A. S. Salama, and K. Hirota, Dual-level template for enhancing resolution of quantum images, Journal of Advanced Computational Intelligence and Intelligent Informatics 26 (2022), no. 3, 431–440.

(Hongkang Ni) Stanford University, Stanford, CA 94305

 $Email\ address{:}\ \texttt{hongkang@stanford.edu}$

(Lexing Ying) Stanford University, Stanford, CA 94305

 $Email\ address{:}\ {\tt lexing@stanford.edu}$